R. & M. No. 2925
(15,499, 16,210)
A.R.C. Technical Report

MINISTRY OF SUPPLY

AERONAUTICAL RESEARCH COUNCIL
REPORTS AND MEMORANDA

Measurements of the Aerodynamic Derivatives for Swept Wings of Low Aspect Ratio describing Pitching and Plunging Oscillations in Incompressible Flow

By

C. SCRUTON, B.Sc., L. WOODGATE, and A. J. ALEXANDER, B.Sc.,
of the Aerodynamics Division, N.P.L.

LONDON: HER MAJESTY'S STATIONERY OFFICE
1957
TEN SHILLINGS NET

Measurements of the Aerodynamic Derivatives for Swept Wings of Low Aspect Ratio describing Pitching and Plunging Oscillations in Incompressible Flow

By

C. SCRUTON, B.Sc., L. WOODGATE, and A. J. ALEXANDER, B.Sc.,
of the Aerodynamics Division, N.P.L.

Reports and Memoranda No 2925*
October, 1953

Summary.—The aerodynamic lift and moment derivatives for pitching oscillations in incompressible flow have been measured for two axis positions on (i) a clipped delta wing of aspect ratio 1·2, (ii) a complete delta wing of aspect ratio 1·6, and (iii) an arrowhead wing of aspect ratio 1·32. The results for the arrowhead wing and the clipped delta wing are compared with values predicted by the vortex-lattice[5] and the Multhopp-Garner[6] methods of calculation. The results for the complete delta wing are compared with values calculated by Garner[6] and by Lawrence and Gerber[11]. In each of the comparisons a satisfactory measure of agreement was found between the theoretical and experimental values of the derivatives. Calculated values for the clipped delta wing based on very low aspect ratio theory[2] did not accord with those found by experiment.

1. *Introduction*.—1.1. *Range and Purpose of the Investigation*.—It has been shown by W. P. Jones[1] that theoretical estimates of flutter and stability derivatives for a wing of finite span in compressible flow can be derived from the solution for an 'equivalent' wing in incompressible flow. One of the requirements for the equivalent wing is that its lateral dimensions should be $(1 - M_0^2)^{1/2}$ times those of the original wing, where M_0 denotes the Mach number of the compressible flow considered. Hence the successful application of the proposed method depends on the reliability of the methods developed for calculating the derivatives of wings of very low aspect ratio oscillating in incompressible flow. The various methods at present available for such calculations include Garrick's[2] extension of R. T. Jones' solution for steady flow, the vortex-lattice method as developed for unsteady flow by W. P. Jones[3] and Lehrian[4,5], the adaptation by Garner[6] of Multhopp's lifting-surface theory to wings oscillating at low frequency, and the method of Lawrence and Gerber[11] for plan-forms with straight trailing edges. The purpose of the experiments to be described was to provide values of the derivatives for comparison with those given by the various theories, and also to determine the influence of mean incidence on the derivatives.

The measurements were made with wings of three plan-forms. These were :

(i) a clipped delta wing with a taper ratio of 1/7, an aspect ratio of 1·2, and a thickness/chord ratio of 0·06 (*see* Fig. 1)

(ii) a complete delta wing of aspect ratio 1·6 obtained by restoring the tips to the clipped delta wing (*see* Fig. 2)

(iii) an arrowhead wing, of aspect ratio 1·32, and thickness/chord ratio 0·10 (*see* Fig. 3)

* Published with permission of the Director, National Physical Laboratory.

For each plan-form the pitching moment and the lift derivatives due to pitching motion were measured directly for two axis positions ; those due to the plunging motion were obtained from these results by the usual transformation formulae[9]. The tests, which covered the range of frequency parameter $0{\cdot}06 < \omega < 0{\cdot}75$, were carried out in the N.P.L. Low Turbulence Wind Tunnel at wind speeds of between 60 and 120 ft per sec. The tunnel had a polygonal working-section with sixteen equal sides, opposite faces being spaced 7 ft apart.

1.2. *Nomenclature for the Aerodynamic Derivatives.*—The sign convention used is shown in the diagrams of Figs. 6 and 7.

The aerodynamic lift and pitching moment, L and M, for plunging and pitching oscillations are expressed in terms of their derivatives by

$$L = L_{\ddot{z}}\ddot{z} + L_{\dot{z}}\dot{z} + L_z z + L_{\ddot{\theta}}\ddot{\theta} + L_{\dot{\theta}}\dot{\theta} + L_\theta\theta \quad \ldots \quad (1)$$

and

$$M = M_{\ddot{z}}\ddot{z} + M_{\dot{z}}\dot{z} + M_z z + M_{\ddot{\theta}}\ddot{\theta} + M_{\dot{\theta}}\dot{\theta} + M_\theta\theta \quad \ldots \quad (2)$$

where $\bar{c}z$ and θ are respectively the vertical translational and the angular displacements of the wing.

For simple harmonic motions of frequency $p/2\pi$, L and M are expressed in terms of their non-dimensional in-phase and out-of-phase components :

$$L = \rho V^2 S[(l_z + i\omega l_{\dot{z}})\, z + (l_\theta + i\omega l_{\dot{\theta}})\theta] \quad \ldots \quad (3)$$

$$M = \rho V^2 S\bar{c}[(m_z + i\omega m_{\dot{z}})\, z + (m_\theta + i\omega m_{\dot{\theta}})\theta] \quad \ldots \quad (4)$$

where $\omega = p\bar{c}/V$.

The dimensional and non-dimensional coefficients are related as follows :

$$\left.\begin{aligned} L_z - p^2 L_{\ddot{z}} &= \rho V^2 S l_z\,; \quad L_{\dot{z}} = \rho V S\bar{c} l_{\dot{z}} \\ L_\theta - p^2 L_{\ddot{\theta}} &= \rho V^2 S l_\theta\,; \quad L_{\dot{\theta}} = \rho V S\bar{c} l_{\dot{\theta}} \\ M_z - p^2 M_{\ddot{z}} &= \rho V^2 S\bar{c} m_z\,; \; M_{\dot{z}} = \rho V S\bar{c}^2 m_{\dot{z}} \\ M_\theta - p^2 M_{\ddot{\theta}} &= \rho V^2 S\bar{c} m_\theta\,; \; M_{\dot{\theta}} = \rho V S\bar{c}^2 m_{\dot{\theta}} \end{aligned}\right\} \quad \ldots \quad (5)$$

The value of the aerodynamic inertia $-\bar{M}_{\ddot{\theta}}$ for pitching oscillations in still air was required for the experiments. It is expressed non-dimensionally as

$$-\bar{m}_{\ddot{\theta}} = -\bar{M}_{\ddot{\theta}}/\rho S\bar{c}^3\,. \quad \ldots \quad (6)$$

1.3. *Construction of the Models.*—The plan-form, section and main dimensions of the wings are shown on Figs. 1, 2 and 3, the RAE 102 section of thickness/chord ratio $0{\cdot}06$ or $0{\cdot}10$ being maintained at all spanwise sections.

The models were built of solid balsa-wood strengthened by a framework of pine. This framework is shown by the broken lines of the drawings, and it included the central box (A) which enclosed the spring hinge used for the pitching axis. All the force-bearing fittings to the wing were attached to the pine framework.

The 8-leaf spring hinge, which spanned the width of the pine-box (A), is illustrated by the photograph of Fig. 5. Its fore-and-aft position was adjustable, and the complete hinge could be rotated at its end fittings to the supports so that the wing could be set to high mean incidences without overstressing the leaf springs. The damping of the wing motion produced by the hinge was negligibly small for most conditions of test.

2. *Methods of Measurement.*—2.1. *The Derivatives m_θ, $m_{\dot\theta}$.*—The two methods used for the measurement of m_θ and $m_{\dot\theta}$ will be described under the headings 'off-resonance' and 'resonance' methods.

(*a*) *Off-resonance Method.*—The apparatus used previously for the experiments described in R. & M. 2373[7] was adapted for the present measurements. It is shown schematically in Fig. 6.

The equation of motion of the wing when forced through the spring S_1 by the sinusoidal motion of the cross-head of amplitude y_0 is given by

$$I\ddot\theta + K\dot\theta + \sigma\theta = M + \sigma_f r y_0' e^{ipt} \quad \ldots \quad (7)$$

where I, K, and σ are respectively the structural inertial, damping and stiffness coefficients.

If the resultant motion of the wing is written

$$\theta = \theta_0 e^{i(pt+\varepsilon)}$$

and M is expanded in terms of its non-dimensional constituents m_θ and $m_{\dot\theta}$ then, for $z = 0$,

$$\left.\begin{aligned} m_\theta &= [(\sigma - Ip^2) - (\sigma_f r y_0 \cos\varepsilon)/\theta_0]/\rho V^2 S\bar{c} \\ \omega m_{\dot\theta} &= [pK + (\sigma_f r y_0 \sin\varepsilon)/\theta_0]/\rho V^2 S\bar{c} \end{aligned}\right\} \quad \ldots \quad (8)$$

In the evaluation of m_θ and $m_{\dot\theta}$ from equations (8) the elastic stiffness σ and σ_f were obtained from static loading tests. $(I - \bar{M}_{\ddot\theta})$ was found from a measurement of the natural frequency of oscillation and a value of $-\bar{M}_{\ddot\theta}$ obtained from bi-plate experiments[8] was subtracted to yield the value of I. The apparatus damping K proved to be very small compared with the wind-on aerodynamic damping to be measured, and therefore very accurate determinations of K were not considered to be necessary. The following approximate method was adopted to expedite the experiments. Values of $K - \bar{M}_{\dot\theta}$ were obtained by decaying oscillation tests in still air. The corresponding values of $-\bar{M}_{\dot\theta}$ were taken to be those of a flat plate of the same plan-form as the wing. They were found by swinging experiments on a rig outside the wind tunnel by taking the difference of the damping values obtained with the flat plate and with a concentrated mass of equivalent inertia substituted for the flat plate. Both $K - \bar{M}_{\dot\theta}$ and $-\bar{M}_{\dot\theta}$ were expressed as linear functions of amplitude, and their difference K also showed some variation with amplitude.

A micrometer method was used to determine the amplitude of the y-motion and also the phase of this motion relative to a datum on a phase-commutator fitted to the driving shaft of the reciprocating gear.

Records of the forced motion were used to determine θ_0 and ε. These records were obtained by photographing the light from a spark (*see* Fig. 6) on a rotating drum camera after reflection from a concave mirror placed in the wing. The sparks occurred between magnesium electrodes in the secondary circuit of an induction coil and were produced at 15-deg phase intervals of the forcing motion by the operation of the phase-commutator. Initially the commutator was contact operated; each contact break triggered a neostron relay circuit which discharged a condenser through the primary winding of the induction coil. Later a more reliable and trouble-free action was obtained by replacing the contact-commutator on the driving shaft by a Tufnol disc carrying small stalloy inserts at phase-intervals of 15 deg. The pulses developed when these inserts swept past the pole-piece of an electro-magnetic pick-up were amplified by a special pulse-shaping amplifier and the output signal produced was used to trigger the neostron relay operating the sparks. A further spark was controlled by an electrically maintained tuning fork and was focussed directly on to the camera drum to provide both a time scale and a datum line. In the analysis average values of the displacement amplitude for corresponding phase angles were taken over ten consecutive cycles and the most probable values of θ_0 and ε were then obtained by a 'least-square' method. A small correction to ε was necessary to allow for the time lag between the contact break and the production of the spark. This lag was measured by observation of the commutator in the light of the spark.

(*b*) *Resonance Method*.—Some initial measurements of m_θ and $m_{\dot\theta}$ were attempted by observation of the resonance frequency $p_r/2\pi$ and the maximum amplitude attained during a resonance test. It was found that the value of p_r could not be estimated with sufficient accuracy to yield reliable values of m_θ, but the values of $m_{\dot\theta}$, given by equation (9) below showed very good agreement with those obtained in the off-resonance tests.

When, as is usual, the difference between the resonance frequency and the natural frequency of oscillation in a wind is small, the following expression yields the value of $m_{\dot\theta}$ to a close approximation :

$$\rho V S \bar{c}^2 m_{\dot\theta} = K - \frac{\sigma_f r y_0}{p_r \theta_{0\,\max}} \left[1 - \frac{\sigma_f{}^2 r^2 y_0{}^2}{8 p_r{}^4 (I - \bar{M}_{\ddot\theta})^2\, \theta_{0\max}{}^2} \right] \quad \ldots \quad (9)$$

2.2. *The Derivatives* l_θ, $l_{\dot\theta}$.—For these measurements the wing was forced inexorably in pitching motion and the amplitude R_0 and the phase ε of the vertical force at the support were determined. The wing was supported at the pitching axis by the vertical force indicator shown in the photographs of Figs. 4 and 5, and to the rear of this position by the rigid link connecting the wing to the eccentric of the driving shaft (Fig. 7). Ball-bearing pivots at both ends of the link allowed the rotation of the shaft to be converted to a sinusoidal pitching motion of the wing with only axial forces in the link.

The hinge was attached to the movable limbs A of the indicator (*see* Fig. 5). The horizontal steel flexure strips B connected the movable to the fixed limbs of the support to give parallel motion and to resist the drag forces. The movement was restrained by the substantial elastic stiffness provided by the semi-circular springs C. Corresponding limbs at each end of the hinge were connected by the cross-bars D. These were bridged at their mid-points by a small concave mirror E supported on vertical flexible phosphor-bronze strips which allowed the mirror to tilt with small differential movements of the cross-bars. Since the mirror was positioned midway between the hinge supports the angle of tilt was independent of the proportion of the total load carried by each support.

In the experiments the wing was forced in pitching motion and the movements of the tilting mirror were recorded by photographing the light from the phase-spark on the drum camera after reflection from the mirror. These records were analyzed in the same way as those described in section 2.1(*a*), and they yielded the amplitude ψ_0 and the phase ε of the tilting motion of the mirror. The elastic stiffness of the vertical motion was calibrated in terms of the vertical load per unit tilt of the mirror by static loading of the hinge axis in still air. To obtain the total effective stiffness σ_v in the wing it was necessary to allow for the restoring action due to the drag forces. This allowance was only significant at the higher wing incidences used in the tests and was calculated from a knowledge of the drag and the length of the horizontal strips B. Finally the value of R_0 was found from the following relation which takes into account the influence of the inertial reactions due to the small vertical movements of the model

$$R_0 = \sigma_v \psi_0 (1 - f^2/f_v{}^2) \quad \ldots \quad (10)$$

where f is the frequency of oscillation of the wing and f_v is the natural frequency in vertical motion of the wing on its spring support.

In the tests the value of σ_v was made sufficiently high to restrict the maximum amplitude of the vertical motion to less than a prescribed limit of 0·01 in. It also gave a high value of f_v so that the factor $(1 - f^2/f_v{}^2)$ did not differ from unity by more than 0·03 in any test.

Since the small vertical movement permitted ensured that the aerodynamic forces and moments due to the vertical motion of the wing were negligible, the balance of the vertical forces is given by

$$W \bar{x} \ddot\theta = -(T + R + L) \quad \ldots \quad (11)$$

and that of the pitching moments with respect to the hinge by

$$I \ddot\theta = -Tr + M - K\theta \quad \ldots \quad (12)$$

Here $W\bar{x}$ and I are respectively the mass moment and the moment of inertia of the system and T and R are the reactions exerted by the forcing link and the hinge support due to the oscillation of the model.

When K is negligibly small and the unknown T is eliminated from the above equations

$$R = (I/r - W\bar{x})\ddot{\theta} - (L + M/r) \quad \ldots \quad (13)$$

the substitution in equation (13) of

$$I' = I/r - W\bar{x}, \quad \theta_0 = \theta_0 \, e^{ipt}, \quad R = R_0 \, e^{i(pt+\varepsilon)}, \quad R_0' = R_0/\theta_0$$

and of the non-dimensional forms of the derivatives yields the following expressions for l_θ and $\omega l_{\dot{\theta}}$:

$$l_\theta = - \left[\frac{R_0' \cos \varepsilon + I'p^2}{\rho V^2 S} + \frac{\bar{c}}{r} \cdot m_\theta \right] \quad \ldots \quad (14)$$

$$\omega l_{\dot{\theta}} = - \left[\frac{R_0' \sin \varepsilon}{\rho V^2 S} + \frac{\bar{c}}{r} \cdot \omega m_{\dot{\theta}} \right] . \quad \ldots \quad (15)$$

The values of m_θ and $m_{\dot{\theta}}$ used in these expressions were supplied by the measurements described in section 2.1.

2.3. *The Derivatives m_z, $m_{\dot{z}}$ and l_z, $l_{\dot{z}}$ and the Position of the Aerodynamic Centre.*—The derivatives of a wing corresponding to two positions of the pitching axis separated by a distance $d\bar{c}$ are related by[9] :

$$\left. \begin{aligned} l_z &= l_z' \\ l_\theta &= l_\theta' + dl_z' \\ m_z &= m_z' - dl_z' \\ m_\theta &= m_\theta' - d(l_\theta' - m_z') - d^2 l_z' \end{aligned} \right\} \quad \ldots \quad (16)$$

where the unaccented symbols refer to the forward axis position. Formulae for the damping derivatives are of the same form. These transformation formulae were used to derive values of m_z, l_z, etc., from the measured values of l_θ, m_θ, etc., obtained with two pitching axes.

The position of the aerodynamic centre is given as a fraction of the mean chord behind the apex of the wing by

$$\bar{h} = h - m_\theta / l_\theta \quad \ldots \quad (17)$$

where the values m_θ, l_θ relate to an axis position $h\bar{c}$ behind the apex. This formula is derived from the last formula in (16) on the assumption that $l_z = m_z = 0$. It is therefore strictly correct only when $\omega = 0$. This estimation of $\bar{h}$ however is only a few per cent in error when $\omega \neq 0$.

3. *Results for a Clipped Delta Wing (Aspect Ratio = 1·2).*—Corrections for tunnel interference were not attempted for this plan-form but it is considered that they would be small.

3.1. *Values for m_θ, $m_{\dot{\theta}}$.*—Measurements of m_θ and $m_{\dot{\theta}}$ were made for a range of ω and α, and for two positions of the pitching axis, $h = 0{\cdot}754$ and $h = 0{\cdot}973$. The results are given in Tables 1 and 2 and those for $\alpha = 0$ are also shown plotted against ω in Fig. 8, together with the theoretical values. The influence of various factors is summarized as follows :

(*a*) *Interference Due to the Model Supports.*—Initially the model support did not extend above the wing (*see* Fig. 6) and it was therefore practicable to suspend a dummy support above the wing to reproduce on the upper surface of the wing similar interference to that produced on the under surface by the true support. Comparison of the results of tests 4 with 7, 6 with 8 (Table 1), and 38 with 41, 40 with 42 (Table 2) show negligible changes due to the added interference. Hence it was inferred that the aerodynamic effects due to the true support could be disregarded.

(*b*) *Amplitude of Oscillation.*—The values of m_θ and $m_{\dot\theta}$ were independent of θ_0 for the test range $0 \cdot 019 < \theta_0 < 0 \cdot 053$ radians. This is shown by the few direct comparisons available (*e.g.*, tests 3 and 4 of Table 1, and 37 to 40 of Table 2) and by the plots of the derivatives against ω in Fig. 8 which permit common curves to be drawn through the points obtained with different amplitudes.

(*c*) *Frequency of Oscillation.*—The derivative values varied little over the test range of ω, but tended to rise as $\omega \to 0$.

Between $\omega = 0 \cdot 16$ and $0 \cdot 7$ the variations of the derivative values are considered to be sufficiently small to justify taking average values as representative for this frequency range. These values are quoted in Table 5.

(*d*) *Scale.*—The Reynolds number for most tests was about $1 \cdot 5 \times 10^6$, corresponding to a wind speed of nearly 120 ft per sec. A few tests made with half these values (*see* Table 1(*b*) and Fig. 8) gave increases in the values of $-m_\theta$ of about 20 per cent, and in those of $-m_{\dot\theta}$ of about 7 per cent.

(*e*) *Incidence.*—The apparatus was not well suited for measurements at incidence, especially when the pitching axis was forward of the aerodynamic centre. The experimental difficulties increased with incidence and it was only practicable to test up to $\alpha = 15$ deg. The detailed results are quoted in Tables 1 and 2, and the values of m_θ and $m_{\dot\theta}$, corresponding to approximately $\omega = 0 \cdot 3$, are plotted against α in Fig. 9. The damping derivative $-m_{\dot\theta}$ shows little variation with incidence. Subsequent measurements of l_θ, described in section 3.2, showed that the marked variation of m_θ with α was not accompanied by any substantial shift of the aerodynamic centre (*see* Table 6).

3.2. *Values for* l_θ, $l_{\dot\theta}$.—The results of the measurements of l_θ and $l_{\dot\theta}$ for a range of ω and α are given in Tables 3 and 4, and those for $\alpha = 0$ are plotted in Figs. 10 and 11 together with the theoretical estimates. The variation of l_θ and $l_{\dot\theta}$ with α for $\omega = 0 \cdot 3$ approximately is shown by Fig. 12. Some comments on the results are given below.

(*a*) *Influence of the Boundary-Layer Transition.*—The first set of values obtained for $l_{\dot\theta}$ with $h = 0 \cdot 973$ appeared to indicate a definite decrease of $l_{\dot\theta}$ as ω tended to zero. In an attempt to find an explanation for this, observations of the boundary-layer transition on the upper surface of the wing were made by the ' china-clay ' method[10] ; and although subsequent repeat measurements did not confirm the decrease of $l_{\dot\theta}$ with ω, it is considered worthwhile recording these observations. The diagrams of Fig. 13 show that, for the steady wing at negative incidences, the boundary layer on the upper surface was laminar except for a region due to the disturbances caused by the supports. For positive incidences the turbulent region gradually extended forward from the trailing edge until at $\alpha = 10$ deg it covered the whole upper surface of the wing. The china-clay method gives no indication of any movement of the transition which might take place during an oscillation. The diagrams obtained with the oscillating wing (Fig. 13(*b*)) merely indicate that the laminar flow region found for the steady wing remained laminar under oscillatory conditions.

The most direct evidence on the influence of the boundary layer was obtained by repeating the measurements in a turbulent airstream, so that the boundary layer over the whole of both surfaces of the wing (as indicated by china-clay experiments) was turbulent. Sufficient local turbulence for this purpose was produced by two ropes of $\frac{1}{4}$-in diameter, spaced 2 in. apart vertically and stretched horizontally across the wind tunnel 6 ft ahead of the apex of the model wing. It was not considered necessary to re-measure m_θ and $m_{\dot\theta}$ for these conditions, and thus, strictly, only values of the derivative combinations $\{l_\theta + (\bar{c}/r)m_\theta\}$ and $\{l_{\dot\theta} + (\bar{c}/r)m_{\dot\theta}\}$* were obtainable (*see* equations (14) and (15)). However, for convenience in the presentation of the results, values of m_θ and $m_{\dot\theta}$ found for undisturbed airflow conditions were substituted to obtain the values of l_θ and $l_{\dot\theta}$ quoted

* In the experiments $c/r = 2$.

in Table 4 and plotted on Fig. 11 for the wing in the turbulent airflow ; and so the *differences* between the values of l_θ and $l_{\dot\theta}$ shown for the two boundary-layer conditions are truly only the differences between the derivative combinations mentioned above. These differences were not considered to be sufficiently large to warrant further measurements with the boundary layer turbulent over the whole wing, and the remaining tests were carried out in the undisturbed airflow.

(*b*) *Amplitude Effects.*—Measurements were made with various amplitudes within the range $0\cdot0270 < 0_0 < 0\cdot0767$ radians. Within this range the values of l_θ and $l_{\dot\theta}$ were independent of θ_0.

(*c*) *Dependence on* ω.—The plots of l_0 and $l_{\dot\theta}$ against ω shown on Figs. 10 and 11 show very little variation of the derivatives for the test range $0\cdot06 < \omega < 0\cdot60$. At the lower end of this range, where the frequency of oscillation was only about $\frac{1}{2}$ cycle per sec, the damping force was too small to measure with accuracy, and the results for $l_{\dot\theta}$ show considerable scatter.

(*d*) *Variation with Incidence.*—The detailed results of the measurements at incidence are included in Tables 3 and 4, and the values of l_θ and $l_{\dot\theta}$ for $\omega = 0\cdot3$ approximately are plotted against α in Fig. 12. Up, to an incidence of 10 deg the values of l_θ were very nearly equal for both axis positions, and increased with α. The results for $\alpha = 15$ deg, however, are surprising in that there is a substantial difference in the value obtained for the two axis positions. A possible explanation of this effect is the establishment of different types of flow for the two axis positions but if this was so, it is remarkable that the position of the aerodynamic centre did not change (*see* Table 6). The nature of the flow was not investigated and no detailed explanation of the effect is offered by the writers.

3.3. *Values for* m_z, $m_{\dot z}$, l_z, $l_{\dot z}$ *and* $\bar h$.—Re-arrangements of equations (16) give the following relations between the derivatives m_z and l_z and the measured derivatives m_θ and l_θ

$$\left.\begin{aligned} l_z &= l_z' = (l_\theta - l_\theta')/d \\ m_z &= m_z' - dl_z' = l_\theta' + (m_\theta - m_\theta'/d) \end{aligned}\right\} \quad \ldots \quad \ldots \quad \ldots \quad \ldots \qquad (18)$$

and similar expressions for the damping derivatives. Values of m_z, l_z, etc. obtained by the substitution of the means of the measured values are given in Table 5. These values do not, of course, make any further basic contribution to the comparison between theory and experiment, since they are found from the measured derivatives by a theoretical relationship. When comparing the theoretical and experimental results quoted in Table 5 it should be noted that the axis positions used were not sufficiently separated to yield accurate values of the derived derivatives. For instance a $+ 1$ and $- 1$ per cent variation applied simultaneously to the values of $l_{\dot\theta}$ measured at the two axis positions produces a ∓ 16 per cent change in the value of $l_{\dot z}$. The unreasonably high values of l_z and m_z quoted for $\alpha = 15$ deg in Table 5 must be regarded as invalid. They arise from the peculiar discrepancy in the measured values of l_θ for the two axis positions. (*See* section 3.2(*d*).)

The positions of the aerodynamic centre $\bar h$ obtained from equation (17) using the mean values of Table 5 are given in Table 6. Measurements at the two axis positions gave the same position to within about 1 per cent, and for $\alpha = 0$ this position agreed well with theoretical predictions. There was a very slight rearward movement of the centre as the incidence increased.

3.4. *Comparisons with Theory.*—Examination of the experimental and theoretical values of m_θ and $m_{\dot\theta}$ presented in Fig. 8, and those of l_θ and $l_{\dot\theta}$ shown in Figs. 10 and 11, and also of the comparisons afforded by Table 5, shows a satisfactory degree of agreement between the measured values and those given by both the vortex-lattice[5] and the Multhopp-Garner[6] methods of calculation. The theory for very low aspect ratio wings given in Ref. 2 was also applied to the clipped delta plan-form. The results are quoted in Table 5, and show that this theory is not applicable to this wing.

4. *Results for theComplete Delta Wing* (*Aspect Ratio* $= 1 \cdot 6$). Measurements on this wing, were made only at zero wing incidence. No calculations of the *complete* delta wing have been made by the vortex-lattice method but comparison is made with theoretical results given by Lawrence and Gerber[11] as well as with those obtained by Garner[6].

4.1. *m_θ, $\bar{h}$ and $m_{\dot\theta}$* (*Table* 7(*a*) *Fig.* 14).—The measured values of m_θ and $\bar{h}$, showed only slight variations with ω and were in good agreement with Garner's calculations[6]. Over the frequency range of the tests the value of $- m_{\dot\theta}$ remained constant at values of between 85 and 90 per cent of those predicted by Lawrence and Gerber[11]*, and were in slightly closer agreement with the values obtained by Garner for $\omega \to 0$.

4.2. *l_θ and $l_{\dot\theta}$* (*Table* 7(*b*) *and Fig.* 15).—The measured lift slope agreed well with that calculated by Garner[6]. Except for the lowest values of ω, where the measurements of $l_{\dot\theta}$ were not reliable, $l_{\dot\theta}$ was independent of ω, its value being approximately 90 per cent of the values given by both Garner[6] and Lawrence and Gerber[11].

5. *Results for the Arrowhead Wing* (*Aspect Ratio* $= 1 \cdot 32$).—With the exception of a few values given in Table 12 the results quoted are not corrected for wall interference and tunnel blockage effects. Approximate estimates[12] of the wall interference indicate that a correction of 6 per cent should be subtracted from the measured value of l_θ to obtain the free-stream value. The correction to m_θ is dependent on axis position and amounts to $- 0 \cdot 010 l_\theta$ and $- 0 \cdot 001 l_\theta$ respectively for axes at $0 \cdot 883\bar{c}$ and $1 \cdot 063\bar{c}$ aft of the apex of the wing. Rather surprisingly, it was found that the corrections to the damping derivatives $l_{\dot\theta}$ and $m_{\dot\theta}$ are negligibly small. For low wing incidences the corrections for tunnel blockage effects are also negligible, and they do not exceed 2 per cent of the air loads (l_θ, $\omega l_{\dot\theta}$, etc.), at $\alpha = 15$ deg.

5.1. *Values for m_θ and $m_{\dot\theta}$*.—The measured values are tabulated in Tables 8 and 9 and are shown plotted against ω in Figs. 16 to 20, together with some theoretical values. A brief discussion of the results follows.

(*a*) *Amplitude Effects*.—Except for $\alpha = 10$ deg, $h = 1 \cdot 063$, it appears that the results were not influenced significantly by amplitude variations within the test range $0 \cdot 023 < \theta_0 < 0 \cdot 066$ radians. For $\alpha = 10$ deg, $h = 1 \cdot 063$, both m_θ and $m_{\dot\theta}$ varied progressively with θ_0 (*cf.* Tests 60 to 64 of Table 9).

(*b*) *Frequency Effects*.—The measured values of m_θ increased with ω by approximately the same amount as predicted by the vortex-lattice calculations (Figs. 16 and 18). With the pitching axis at $h = 0 \cdot 883$ a slight increase of $- m_{\dot\theta}$ as $\omega \to 0$ also corresponded roughly to that predicted by the calculations (Fig. 17) but for $h = 1 \cdot 063$ the increase was much more rapid than that predicted theoretically (Fig. 19).

(*c*) *Incidence Effects*.—Plots of m_θ and $- m_{\dot\theta}$ for $\omega = 0 \cdot 3$ against α are given in Fig. 20. The values of m_θ for both axis positions decreased considerably at the higher incidences but the corresponding rearward movement of the aerodynamic centre $\bar{h}$ (*see* penultimate column of Table 12) was considerably lessened by increased values of l_θ (*see* Fig. 25).

5.2. *Values for l_θ and $l_{\dot\theta}$*.—The results for l_θ and $l_{\dot\theta}$ are given in Tables 10 and 11 and are plotted in Figs. 21 to 25 together with the calculated values. It should be noted that the accuracy of measurement of l_θ improved, while that of $l_{\dot\theta}$ deteriorated, as the frequency decreased.

(*a*) *Amplitude Effects*.—The result of tests made with $\theta_0 = 0 \cdot 028$ and $0 \cdot 053$ (Tests 74 to 84, Table 10) show no significant effect due to this change of amplitude.

(*b*) *Frequency Effects*.—Except for $\alpha = 15$ deg only slight variations of the values of l_θ and $l_{\dot\theta}$ with ω were found, these usually followed the trend predicted by the vortex-lattice calculations.

---

* The values quoted in this report for a triangular wing of aspect ratio $1 \cdot 6$ were obtained by interpolation of the values given in Ref. 11 for aspect ratios of $0 \cdot 5$, $1 \cdot 0$, $2 \cdot 0$, and $4 \cdot 0$.

(c) *Incidence Effects.*—The variation of l_θ and $l_{\dot\theta}$ for $\omega = 0 \cdot 3$ is shown on Fig. 25. The increases of l_θ found at the higher incidences, and their influence on the aerodynamic centre, have been discussed in section 5.1(c). The value of $l_{\dot\theta}$ changed rapidly with incidence and for both axis positions $l_{\dot\theta}$ would have become negative at incidences a little higher than 15 deg.

5.3. *Influence of the Boundary Layer.*—Observations of the boundary layer over the clipped delta wing tested previously showed that a laminar boundary layer extended over most of the wing surface. Similar observations were not made on the arrowhead wing since it was considered that the same type of flow would exist. In order to assess the effect of considerable changes in the condition of the boundary layer, some measurements were repeated with the model in the turbulent wake produced by two ropes of $\frac{1}{4}$ in. diameter, spaced two inches apart vertically, and stretched horizontally across the tunnel 6 ft ahead of the model. The presence of these ropes, which must have produced a turbulent boundary layer existing over the whole wing, had negligible effect on l_θ and $l_{\dot\theta}$ (Figs. 21 and 22). The changes found in the values of m_θ and $m_{\dot\theta}$ were less than 10 per cent.

5.4. *Comparisons with Theory.*—Comparative theoretical and experimental values are shown on the graphs of Figs. 16 to 19 and 21 to 24. The values plotted in these figures are all uncorrected for wind-tunnel interference effects. Approximate estimates of the corrections to be applied are given in section 5. In Table 12 some corrected results are given for zero mean incidence and $\omega = 0 \cdot 3$, and the comments which follow refer to the comparison between the calculated values and those given by tests carried out with zero mean incidence.

(a) *m_θ and h.*—Vortex-lattice theory[5] predicted accurately the trend of variation of m_θ with ω (Figs. 16 and 18). Both pitching axes used in the tests were close to the aerodynamic centre of the wing and hence the considerable percentage differences between the calculated and the measured values of m_θ are not very significant. If the results quoted in Table 12 are referred to a pitching axis at the apex of the wing then for $\omega = 0 \cdot 3$ the vortex-lattice method yields $m_\theta = -0 \cdot 763$ and the value derived from the corrected experimental results becomes $m_\theta = -0 \cdot 750$. The corresponding value given by the Multhopp-Garner calculations for $\omega \rightarrow 0$ is $-0 \cdot 809$. The experimental value quoted above cannot be regarded as very reliable since the pitching axes used in the tests were insufficiently separated for accurate extrapolation to an axis at the apex of the wing. The position of the aerodynamic centre $\bar{h}$ (Table 12) was predicted more accurately by the Multhopp-Garner method.

(b) *$m_{\dot\theta}$.*—The measured values of $-m_{\dot\theta}$ were in general somewhat lower than the theoretical estimates (Figs. 17 and 19). This does not apply for low values of ω with $h = 1 \cdot 063$ when the experimental values of $-m_{\dot\theta}$ increased rapidly as $\omega \rightarrow 0$. For $\omega = 0 \cdot 3$ the ratio of the measured to the calculated (vortex-lattice) values is $0 \cdot 82$ for the rear, and $0 \cdot 94$ for the forward, axis positions.

(c) *l_θ.*—The mean of the measured values of l_θ after correction for tunnel interference is about 10 per cent higher than the calculated values (Figs. 21 and 23).

(d) *$l_{\dot\theta}$.*—Theory and experiment showed very good agreement for the forward position of the pitching axis (Fig. 22), especially at the higher frequencies. For the rear position (Fig. 24) the measured values varied between 84 to 92 per cent of those calculated, the closer agreement being found at the higher frequencies.

6. *Conclusions.*—In the experiments described the aerodynamic lift and moment derivatives have been measured on a clipped delta wing, a complete delta wing and an arrowhead wing. For all three plan-forms values calculated by the Multhopp-Garner method[6] are available for comparison with the measured values. Calculations by the vortex-lattice method[5] have been made for the clipped delta and arrowhead but not for the complete delta plan-forms. Lawrence and Gerber[11] quote calculated values for the complete delta (and rectangular) wings only. In each of the above available comparisons the agreement found between the predicted and the measured

values is considered to be fairly satisfactory. No one of these three theoretical treatments consistently yields results of better agreement with experiment than the other two. For the clipped delta wing comparison was also made between measured values and those given by the low aspect ratio of Ref. 2. Values calculated by this theory were not confirmed by the experiments.

NOTATION

$\bar{c}$		Mean chord of wing
c_0		Root chord of wing
$d\bar{c}$		Distance between two positions of the pitching axis
f		Frequency of the pitching oscillation
f_v		Natural frequency in vertical motion of the wing mounted on the vertical force indicator
$h\bar{c}$		Distance between the pitching axis and the apex of the wing
$\bar{h}\bar{c}$		Distance of the aerodynamic centre from the apex of the wing
I		Structural moment of inertia of the wing
K		'Apparatus' damping of the wing on its mounting
L, M		Respectively the increments of the aerodynamic lift and pitching moment due to oscillation of the wing
L_z, L_θ, M_z, M_θ, etc.		Aerodynamic lift and pitching-moment derivatives (defined in section 1.2)
l_z, l_θ, m_z, m_θ, etc.		Non-dimensional forms of these derivatives (defined in section 1.2)
p	=	$2\pi f$
p_r	=	$2\pi \times$ frequency at resonance
R_e	=	$V\bar{c}/\nu$
R, R_0		Increment of the vertical force at the hinge and its amplitude due to the oscillation
S		Area of the wing plan-form
r		Moment arm of the forcing motion
t		Time
V		Wind velocity
W		Mass of model
$\bar{x}$		Distance of the centre of gravity of the model wing aft of the pitching axis
y_0		Linear amplitude of the forcing motion
$z\bar{c}$		Vertical displacement of the reference axis
α		Mean incidence

NOTATION—*continued*

ε		Phase advance of the response to sinusoidal excitation
θ, θ_0		Angular displacement of the wing in pitching oscillation, and its amplitude
ν		Kinematic viscosity of air
σ, σ_f, σ_v		Elastic stiffnesses
ψ_σ		Amplitude of tilt of the vertical force indicator mirror
ω	=	$p\bar{c}/V$
ρ		Air density

REFERENCES

No.	Author	Title, etc.
1	W. P. Jones	Oscillating wings in compressible subsonic flow. R. & M. 2855. October, 1951.
2	I. E. Garrick	Some research on high-speed flutter. Proceedings of the Third Anglo-American Aeronautical Conference, 1951. Royal Aeronautical Society.
3	W. P. Jones	The calculation of aerodynamic derivative coefficients for wings of any plan form in non-uniform motion. R. & M. 2470. December, 1946.
4	D. E. Lehrian	Aerodynamic coefficients for an oscillating delta wing. R. & M. 2841 July, 1951.
5	D. E. Lehrian	Calculation of flutter derivatives for wings of general plan form. A.R.C. 16,445. January, 1954. (Unpublished.)
6	H. C. Garner	Multhopp's subsonic lifting surface theory of wings in slow pitching oscillations. R. & M. 2885. July, 1952.
7	C. Scruton, W. G. Raymer and D. V. Dunsdon	Experimental determination of the aerodynamic derivatives for flexural-aileron flutter of B.A.C. wing type 167. R. & M. 2373. May, 1945.
8	C. Scruton	Some experimental determinations of the apparent additional mass effect for an aerofoil and for flat plates. R. & M. 1931. October, 1941.
9	W. J. Duncan and A. R. Collar ..	Calculation of the resistance derivatives of flutter theory. Part I. R. & M. 1500. October, 1932.
10	E. J. Richards and F. H. Burstall ..	The 'china-clay' method of indicating transition. R. & M. 2126. August, 1945.
11	H. R. Lawrence and E. H. Gerber ..	The aerodynamic forces on low aspect ratio wings oscillating in an incompressible flow. *J.Ae.Sci.*, Vol. 19, No. 11, pp. 769 to 781. November, 1952.
12	W. E. Acum and H. C. Garner ..	Approximate wall corrections for an oscillating swept wing in a wind tunnel of closed circular section. A.R.C. 16,512. January, 1954. (Unpublished.)

TABLE 1

Results for the Clipped Delta Wing. Aspect ratio = 1·2.

Variation of m_θ and $m_{\dot\theta}$ with ω and α for a Pitching Axis $0 \cdot 745\bar{c}$ from the Apex

(a) $V = 118 \cdot 6$ ft/sec ; $R_e = 1 \cdot 5 \times 10^6$; $\bar{m}_{\ddot\theta} = 0 \cdot 129$

Test No.	α (deg)	ω	θ_0 (radians)	$-m_\theta$	$-m_{\dot\theta}$
1	0	0·154	0·0225	0·194	0·496
2	0	0·230	0·0194	0·198	0·500
3	0	0·324	0·0281	0·198	0·484
4	0	0·322	0·0181	0·198	0·483
5	0	0·410	0·0327	0·193	0·488
6	0	0·440	0·0229	0·190	0·486
7*	0	0·328	0·0280	0·201	0·485
8*	0	0·440	0·0346	0·207	0·492
9	+3·9	0·209	0·0144	0·266	0·525
10	+3·9	0·321	0·0245	0·262	0·493
11	+3·9	0·412	0·0283	0·250	0·504
12	−5	0·156	0·0196	0·349	0·508
13	−5	0·164	0·0204	0·337	0·507
14	−5	0·214	0·0183	0·345	0·491
15	−5	0·314	0·0277	0·328	0·470
16	−5	0·420	0·0328	0·312	0·477
17	−10	0·158	0·0205	0·443	0·548
18	−10	0·216	0·0219	0·437	0·534
19	−10	0·314	0·0245	0·430	0·513
20	−10	0·476	0·0292	0·435	0·486
21	−15	0·218	0·0255	0·521	0·547
22	−15	0·320	0·0290	0·470	0·522
23	−15	0·412	0·0336	0·435	0·552
(b) $V = 59 \cdot 25$ ft/sec ; $R_e = 0 \cdot 75 \times 10^6$					
24	0	0·161	0·0213	0·239	0·539
25	0	0·223	0·0255	0·235	0·512
26	0	0·331	0·0189	0·247	0·525
27	0	0·664	0·0308	0·254	—

* These tests were made with a dummy support suspended above the wing to form a 'mirror image' of the true support with respect to the horizontal plane of the wing.

TABLE 2

Results for the Clipped Delta Wing. Aspect Ratio $= 1\cdot2$.

Variation of m_θ *and* $m_{\dot\theta}$ *with* ω *and* α *for a Pitching Axis* $0\cdot973\bar{c}$ *for the Apex*

$V = 118\cdot6$ ft/sec ; $R_e = 1\cdot5 \times 10^6$; $-\bar{m}_{\dot\theta} = 0\cdot050$.

Test No.	α (deg)	ω	θ_0 (radians)	$-m_\theta$	$-m_{\dot\theta}$
28	0	0·106	0·0309	0·0122	0·294
29		0·159	0·0311	0·0134	0·272
30		0·300	0·0280	0·0071	0·269
31*		0·341	0·0278	—	0·262
32		0·403	0·0278	0·0100	0·263
33		0·413	0·0351	0·0081	0·255
34*		0·498	0·0420	—	0·263
35*		0·514	0·0378	—	0·271
36		0·526	0·0385	−0·0037	0·273
37*		0·646	0·0303	—	0·262
38*		0·658	0·0368	—	0·263
39*		0·670	0·0188	—	0·255
40*		0·681	0·0520	—	0·252
41+*		0·659	0·0298	—	0·261
42+*		0·684	0·0523	—	0·252
43	+5	0·163	0·0155	0·0830	0·285
44		0·260	0·0231	0·0769	0·274
45		0·342	0·0216	0·0842	0·251
46		0·398	0·0251	0·0798	0·252
47	−5	0·187	0·0144	0·0908	0·305
48		0·273	0·0201	0·0834	0·278
49		0·314	0·0189	0·0898	0·256
50		0·416	0·0247	0·0785	0·258
51	−8	0·173	0·0098	0·1495	0·241
52		0·275	0·0222	0·1565	0·249
53		0·307	0·0199	0·1462	0·244
54		0·415	0·0261	0·1226	0·247
55	−10	0·311	0·0204	0·1351	0·279
56		0·411	0·0263	0·1180	0·281
57	−15	0·300	0·0230	0·1090	0·311
58		0·422	0·0305	0·0812	0·334

* Values obtained from the resonance method (*see* section 2.1(*b*)).

+ See footnote to Table 1.

TABLE 3

Results for the Clipped Delta Wing. Aspect Ratio $= 1 \cdot 2$.

Variation of l_θ *and* $l_{\dot\theta}$ *with* ω *and* α *for a Pitching Axis at* $h = 0 \cdot 754$

$V = 108 \cdot 6$ ft/sec ; $R_e = 1 \cdot 4 \times 10^6$.

Test No.	α (deg)	ω	θ_0 (radians)	l_θ	$l_{\dot\theta}$
59		0·055	0·0544	0·841	0·891
60		0·113	0·0544	0·836	0·916
61		0·232	0·0544	0·839	0·991
62		0·360	0·0544	0·843	1·018
63		0·468	0·0544	0·855	1·017
64	0	0·576	0·0544	0·947	1·016
65		0·119	0·0705	0·833	0·972
66		0·237	0·0705	0·837	0·996
67		0·465	0·0705	0·860	1·011
68		0·567	0·0705	0·884	1·017
69		0·115	0·0716	1·102	1·003
70	−5	0·237	0·0716	1·073	1·001
71		0·403	0·0716	1·050	0·976
72		0·583	0·0716	1·041	0·930
73		0·117	0·0728	1·279	0·893
74	−10	0·243	0·0728	1·310	0·943
75		0·400	0·0728	1·318	0·905
76		0·567	0·0728	1·358	0·848
77		0·123	0·0751	1·39	0·723
78	−15	0·245	0·0751	1·42	0·833
79		0·410	0·0751	1·47	0·823
80		0·579	0·0751	1·54	0·854

TABLE 4

Results for the Clipped Delta Wing. Aspect Ratio $= 1\cdot2$.
Variation of l_θ *and* $l_{\dot\theta}$ *with* ω *and* α *for a Pitching Axis at* $h = 0\cdot973$

$V = 108\cdot6$ ft/sec ; $R_e = 1\cdot4 \times 10^6$

Test No.	α (deg)	ω	θ_0 (radians)	l_θ	$l_{\dot\theta}$
81		0·056	0·0270	0·870	1·085
82		0·066	0·0270	0·825	0·789
83		0·088	0·0270	0·826	0·804
84		0·090	0·0270	0·844	0·794
85	0	0·115	0·0270	0·845	0·877
86		0·176	0·0270	0·849	0·870
87		0·235	0·0270	0·851	0·852
88		0·344	0·0270	0·854	0·833
89		0·475	0·0270	0·839	0·857
90		0·561	0·0270	0·837	0·858
91		0·061	0·0529	0·850	0·754
92		0·066	0·0529	0·857	1·016
93		0·074	0·0529	0·857	0·904
94	0	0·117	0·0529	0·856	0·867
95		0·224	0·0529	0·850	0·812
96		0·553	0·0529	0·844	0·826
97*		0·070	0·0529	0·913	0·723
98*		0·124	0·0529	0·907	0·826
99	0	0·243	0·0529	0·866	0·814
100*		0·366	0·0529	0·909	0·822
101*		0·593	0·0529	0·923	0·822
102		0·059	0·0767	0·846	0·915
103		0·080	0·0767	0·842	0·931
104		0·115	0·0767	0·850	0·878
105	0	0·178	0·0767	0·859	0·893
106		0·234	0·0767	0·856	0·749
107		0·366	0·0767	0·859	0·865
108		0·468	0·0767	0·852	0·855
109		0·616	0·0767	0·863	0·859
110		0·112	0·0565	1·014	0·706
111		0·175	0·0565	1·023	0·814
112		0·243	0·0565	1·013	0·779
113	−5	0·354	0·0565	1·021	0·755
114		0·449	0·0565	1·015	0·761
115		0·544	0·0565	1·133	0·765
116		0·237	0·0541	1·276	0·606
117		0·354	0·0541	1·280	0·646
118	−10	0·464	0·0541	1·286	0·677
119		0·573	0·0541	1·288	0·677
120		0·232	0·0557	0·888	0·463
121		0·347	0·0557	0·842	0·573
122	−15	0·470	0·0557	0·790	0·577
123		0·574	0·0557	0·785	0·639
124		0·620	0·0557	0·699	0·624

* These tests were carried out with the model in the disturbed flow caused by two ropes stretched horizontally across the tunnel 6 ft ahead of the model and spaced 2 in. apart vertically. The turbulent boundary layer then extended over the whole wing.

TABLE 5

Results for the Clipped Delta Wing.

Mean Values of the Derivatives, and the Comparative Theoretical Values

---

The values quoted below for l_θ, $l_{\dot\theta}$, m_θ $m_{\dot\theta}$ are the means taken over the ω range tested. These derivatives did not vary significantly with ω except for some instances at the higher incidences. For this reason the values given below may differ slightly from those plotted in Figs. 9 and 12 for $\omega = 0{\cdot}3$.

The derived derivatives l_z, $l_{\dot z}$, m_z and $m_{\dot z}$ and the derivative values quoted for $h = 0$, were obtained from these mean values by equations (16).

The calculated values quoted for the vortex-lattice method relate to $\omega = 0{\cdot}3$.

h	α	l_z	$l_{\dot z}$	l_θ	$l_{\dot\theta}$	m_z	$m_{\dot z}$	m_θ	$m_{\dot\theta}$	Method
		0	0·812	0·812	1·662	0	−0·797	−0·797	−1·870	Multhopp-Garner
		−0·036	0·805	0·771	1·571	0·044	−0·774	−0·774	−1·788	Vortex-lattice
		0	0·942	0·942	2·353	0	−0·942	−0·942	−2·89	Ref. 2
0	0	0	0·552	0·856	1·404	0	−0·574	−0·831	−1·667	Experiment
	5	0·142	0·985	1·174	1·720	−0·204	−0·980	−1·291	−1·970	
	10	0·157	1·12	1·435	1·741	−0·262	−1·287	−1·622	−2·167	
	15	3·00	1·07	3·71	1·616	−3·21	−1·232	−3·99	−2·08	
		0	0·812	0·812	1·050	0	−0·185	−0·185	−0·476	Multhopp-Garner
		−0·036	0·805	0·798	0·964	0·017	−0·166	−0·155	−0·477	Vortex-lattice
		0	0·942	0·942	1·643	0	−0·232	−0·232	−0·934	Ref. 2
0·754	0	0	0·552	0·856	0·988	0	−0·157	−0·195	−0·489	Experiment
	5	0·142	0·985	1·066	0·977	−0·097	−0·237	−0·334	−0·491	
	10	0·157	1·12	1·316	0·897	−0·143	−0·443	−0·436	−0·520	
	15	3·00	1·07	1·45	0·808	−0·950	−0·425	−0·475	−0·540	
		0	0·812	0·812	0·872	0	−0·007	−0·007	−0·245	Multhopp-Garner
		−0·036	0·805	0·805	0·788	0·010	0·010	0·017	−0·269	Vortex-lattice
		0	0·942	0·942	1·436	0	−0·025	−0·025	−0·560	Ref. 2
0·973	0	0	0·552	0·850	0·867	0	−0·036	−0·008	−0·265	Experiment
	5	0·142	0·985	1·035	0·763	−0·066	−0·023	−0·086	−0·274	
	10	0·157	1·12	1·282	0·652	−0·109	−0·198	−0·127	−0·280	
	15	3·00	1·07	0·800	0·575	−0·299	−0·192	−0·095	−0·323	

TABLE 6

Results for the Clipped Delta Wing:
Position of the Aerodynamic Centre

$\bar{h}\bar{c}$ = distance of the aerodynamic centre from the apex.

α (deg)	Aerodynamic centre $\bar{h}$			
	Experimental		Theoretical	
	Axis at $h = 0\cdot754$	Axis at $h = 0\cdot973$	Multhopp-Garner	Vortex-lattice
0	0·982	0·982	0·982	1·005
5	1·067	1·056	—	—
10	1·085	1·072	—	—
15	1·082	1·082	—	—

Note.—These values of $\bar{h}$ were given by the mean values of m_θ and l_θ quoted in Table 5. They do not differ by more than 2 per cent from those given by values of l_θ and m_θ taken from Figs. 9 and 12 for $\omega = 0\cdot3$.

B

TABLE 7

Results for the Delta Wing. Aspect Ratio = 1·60.

Variation of m_θ, $m_{\dot\theta}$, l_θ *and* $l_{\dot\theta}$ *with* ω
for Pitching Axes at h = 0·862 *and* 1·112

(*a*) Variation of m_θ and $m_{\dot\theta}$ with ω

V = 118·6 ft/sec ; $R_e = 1 \cdot 2 \times 10^6$; α = 0 deg

Test No.	h	ω	θ_0 (radians)	m_θ	$m_{\dot\theta}$	$\bar{h}$* (ω = 0·3)
1		0·096	0·034	−0·362	−0·682	
2		0·184	0·037	−0·359	−0·674	
3	0·862	0·277	0·043	−0·353	−0·678	1·222
4		0·373	0·053	−0·339	−0·678	
5		0·459	0·062	−0·320	−0·682	
6		0·046	0·036	−0·098	−0·348	
7		0·093	0·036	−0·099	−0·352	
8		0·134	0·039	−0·098	−0·355	
9		0·182	0·043	−0·098	−0·351	
10		0·228	0·047	−0·098	−0·350	
11		0·274	0·053	−0·096	−0·352	
12	1·112	0·326	0·043	−0·098	−0·358	1·211
13		0·366	0·025	−0·092	−0·357	
14			0·049	−0·096	−0·356	
15		0·413	0·053	−0·092	−0·357	
16		0·459	0·027	−0·084	−0·357	
17			0·053	−0·089	−0·355	
18		0·522	0·041	−0·079	−0·358	

* Multhopp-Garner calculations yield $\bar{h}$ = 1·205.

(*b*) Variation of l_θ and $l_{\dot\theta}$ with ω

V = 108·6 ft/sec ; $R_e = 1 \cdot 1 \times 10^6$; α = 0 deg

Test No.	h	ω	θ_0 (radians)	l_θ	$l_{\dot\theta}$
19		0·103	0·082	0·983	1·122
20		0·206	,,	0·979	1·187
21	0·862	0·304	,,	0·972	1·191
22		0·403	,,	0·971	1·189
23		0·506	,,	0·960	1·183
24		0·052	0·082	0·979	0·744
25		0·102	,,	0·979	0·863
26	1·112	0·200	,,	0·979	0·929
27		0·300	,,	0·980	0·946
28		0·400	,,	0·982	0·947
29		0·502	,,	0·964	0·953

TABLE 8

Results for the Arrowhead Wing. Aspect Ratio = 1·32.

Variation of m_θ and $m_{\dot{\theta}}$ with ω and α for a Pitching Axis at h = 0·883

$V = 118{\cdot}6$ ft/sec ; $R_e = 1{\cdot}7 \times 10^6$; $-\bar{m}_{\dot{\theta}} = 0{\cdot}083$.

Test No.	α (deg)	ω	θ_0 (radians)	m_θ	$m_{\dot{\theta}}$
1		0·068	0·029	−0·136	−0·262
2		0·149	0·034	−0·142	−0·237
3		0·188	0·034	−0·138	−0·278
4		0·196	0·023	−0·131	−0·277
5		0·247	0·030	−0·127	−0·274
6		0·260	0·042	−0·129	−0·265
7	0	0·316	0·056	−0·127	−0·260
8		0·328	0·078	−0·130	−0·273
9		0·334	0·043	−0·126	−0·272
10		0·337	0·030	−0·126	−0·271
11		0·380	0·058	−0·124	−0·265
12		0·462	0·061	−0·111	−0·267
13		0·519	0·054	−0·111	−0·261
14		0·621	0·057	−0·098	−0·262
15		0·071	0·044	−0·154	−0·313
16		0·138	0·049	−0·153	−0·311
17		0·202	0·052	−0·153	−0·303
18		0·279	0·053	−0·151	−0·298
19	5	0·304	0·061	−0·148	−0·292
20		0·335	0·059	−0·161	−0·293
21		0·382	0·059	−0·144	−0·306
22		0·472	0·063	−0·127	−0·306
23		0·512	0·057	−0·142	−0·297
24		0·638	0·062	−0·123	−0·296
25		0·271	0·048	−0·259	−0·269
26		0·325	0·064	−0·250	−0·274
27	10	0·377	0·054	−0·249	0·263
28		0·538	0·051	−0·241	−0·275
29		0·675	0·061	−0·193	−0·284
30		0·523	0·063	−0·329	−0·229
31	15	0·673	0·039	−0·344	−0·204
32*		0·272	0·049	−0·123	−0·249
33*	0	0·374	0·064	−0·117	−0·251
34*		0·550	0·062	−0·094	−0·235

* These tests were carried out with the model in the disturbed flow caused by two ropes stretched horizontally across the tunnel 6 ft ahead of the model. The turbulent boundary layer then extended over the whole wing.

TABLE 9

Results for the Arrowhead Wing. Aspect Ratio $= 1 \cdot 32$.

Variation of m_θ *and* $m_{\dot\theta}$ *with* ω *and* α
for a Pitching Axis at $h = 1 \cdot 063$

$V = 118 \cdot 6$ ft/sec ; $R_e = 1 \cdot 7 \times 10^6$; $-\bar{m}_{\theta} = 0 \cdot 048$

Test No.	α (deg)	ω	θ_0 (radians)	m_θ	$m_{\dot\theta}$
35		0·027	0·057	0·047	−0·196
36		0·055	0·062	0·048	−0·184
37		0·127	0·046	0·045	−0·165
38		0·149	0·051	0·044	−0·146
39		0·152	0·040	0·053	−0·141
40		0·186	0·058	0·048	−0·138
41	0	0·194	0·023	0·054	−0·137
42		0·247	0·056	0·049	−0·144
43		0·318	0·065	0·048	−0·135
44		0·392	0·047	0·051	−0·135
45		0·473	0·056	0·061	−0·135
46		0·634	0·043	0·069	−0·138
47		0·029	0·024	0·033	−0·174
48		0·060	0·026	0·033	−0·170
49		0·126	0·044	0·037	−0·171
50		0·161	0·042	0·037	−0·170
51	5	0·219	0·039	0·038	−0·167
52		0·317	0·055	0·033	−0·156
53		0·374	0·056	0·032	−0·154
54		0·485	0·054	0·035	−0·152
55		0·654	0·037	0·048	−0·152
56		0·198	0·033	−0·055	−0·121
57		0·233	0·047	−0·043	−0·123
58		0·236	0·057	−0·034	−0·146
59		0·311	0·066	−0·040	−0·137
60		0·345	0·031	−0·063	−0·113
61	10	0·348	0·041	−0·044	−0·123
62		0·349	0·034	−0·048	−0·115
63		0·353	0·066	−0·028	−0·136
64		0·360	0·090	−0·030	−0·138
65		0·426	0·056	−0·026	−0·138
66		0·515	0·055	−0·025	−0·137
67		0·626	0·059	+0·001	−0·141
68		0·314	0·040	−0·138	−0·063
69		0·358	0·062	−0·120	−0·108
70	15	0·437	0·058	−0·119	−0·108
71		0·500	0·058	−0·107	−0·113
72		0·559	0·055	−0·097	−0·110
73		0·666	0·056	−0·084	−0·119

TABLE 10

Results for the Arrowhead Wing. Aspect Ratio = 1·32.

Variation of l_θ and $l_{\dot\theta}$ with ω and α for a Pitching Axis at $h = 0{\cdot}883$

$V = 108{\cdot}6$ ft/sec ; $R_e = 1{\cdot}5 \times 10^6$

Test No.	α (deg)	ω	θ_0 (radians)	l_θ	$l_{\dot\theta}$
74		0	0·058	0·980	—
75		0·071	0·053	0·974	0·831
76		0·143	,,	0·975	0·829
77		0·285	,,	0·953	0·761
78		0·420	,,	0·926	0·772
79	0	0·566	,,	0·904	0·766
80		0·707	,,	0·868	0·758
81		0·139	0·028	0·997	0·604
82		0·285	,,	0·977	0·755
83		0·549	,,	0·945	0·753
84		0·709	,,	0·922	0·759
85		0·141	0·054	0·927	0·694
86	5	0·282	,,	0·918	0·735
87		0·557	,,	0·875	0·761
88		0·701	,,	0·810	0·779
89		0·143	0·055	1·203	0·907
90	10	0·278	,,	1·186	0·823
91		0·556	,,	1·193	0·825
92		0·695	,,	1·180	0·826
93		0·296	0·048	1·288	0·387
94	15	0·518	,,	1·376	0·413
95		0·665	,,	1·498	0·474
96*		0·071	0·053	0·950	0·921
97*		0·146	,,	0·946	0·866
98*	0	0·295	,,	0·935	0·748
99*		0·437	,,	0·922	0·748
100*		0·735	,,	0·855	0·746

* See footnote to Table 8.

TABLE 11

Results for the Arrowhead Wing. Aspect Ratio = 1·32.

Variation of l_θ and $l_{\dot\theta}$ with ω and α for a Pitching Axis at h = 1·063

$V = 108{\cdot}6$ ft/sec ; $R_e = 1{\cdot}5 \times 10^6$

Test No.	α (deg)	ω	θ_0 (radians)	l_θ	$l_{\dot\theta}$
101		0	0·057	1·062	—
102		0·070	,,	1·000	0·553
103		0·137	,,	1·002	0·538
104	0	0·286	,,	1·013	0·554
105		0·416	,,	0·964	0·559
106		0·563	,,	0·973	0·566
107		0·697	,,	1·007	0·580
108		0	0·054	0·976	—
109		0·070	,,	0·933	0·627
110		0·141	,,	0·960	0·604
111	5	0·282	,,	0·983	0·587
112		0·417	,,	0·996	0·574
113		0·567	,,	0·954	0·569
114		0·703	,,	1·003	0·588
115		0	0·055	1·089	—
116		0·284	,,	1·110	0·424
117	10	0·417	,,	1·128	0·435
118		0·578	,,	1·112	0·465
119		0·718	,,	1·160	0·487
120		0	0·057	1·281	—
121		0·280	,,	1·229	0·064
122	15	0·443	,,	1·235	0·136
123		0·544	,,	1·229	0·191
124		0·710	,,	1·293	0·230

TABLE 12

Results for the Arrowhead Wing. Aspect Ratio = 1·32.

Comparison of the Calculated and Measured Values of the Derivatives

The measured values of l_θ, $l_{\dot\theta}$, m_θ and $m_{\dot\theta}$ quoted are those corresponding to $\omega = 0\cdot3$, $\alpha = 0$ deg. The usual transformation formulae (equations (16)) were used to derive the remaining derivatives. The figures in parentheses apply to free-stream conditions and were obtained by using the wall interference corrections calculated by Acum and Garner. These corrections to the damping derivatives were negligible. The values given by the vortex-lattice calculations relate to $\omega = 0\cdot303$.

h	α	l_z	$l_{\dot z}$	l_θ	$l_{\dot\theta}$	m_z	$m_{\dot z}$	m_θ	$m_{\dot\theta}$	$\bar h$	Method
	—	0	0·822	0·822	0·820	0	−0·083	−0·085	−0·286	0·987	Multhopp-Garner
	—	−0·011	0·822	0·820	0·766	+0·007	−0·060	−0·053	−0·286	0·948	Vortex-lattice
0·883	0	−0·195	1·223	0·950	0·770	+0·008	−0·189	−0·128	−0·268	1·018	Experimental
		(−0·183)		(0·893)		(0)		(−0·118)		(1·015)	
	5	−0·278	0·845	0·920	0·735	−0·035	−0·206	−0·149	−0·299	1·045	
	10	+0·473	2·209	1·195	0·820	−0·118	−0·310	−0·255	−0·269	1·096	
	15	+0·306	1·767	1·285	0·390	−0·048	−0·534	−0·360	−0·215	1·163	
	—	0	0·822	0·822	0·672	0	+0·065	+0·063	−0·150	0·987	Multhopp-Garner
	—	−0·011	0·822	0·824	0·618	+0·005	+0·088	+0·094	−0·164	0·948	Vortex-lattice
1·063	0	−0·195	1·223	0·985	0·550	−0·030	+0·031	+0·048	−0·135	1·014	Experimental
		(−0·183)		(0·926)		(−0·030)		(+0·047)		(1·012)	
	5	−0·278	0·845	0·970	0·583	−0·085	−0·054	+0·032	−0·157	1·030	
	10	+0·473	2·209	1·110	0·423	−0·033	0·087	−0·034	−0·137	1·094	
	15	+0·306	1·767	1·230	0·072	+0·007	−0·216	−0·130	−0·106	1·169	

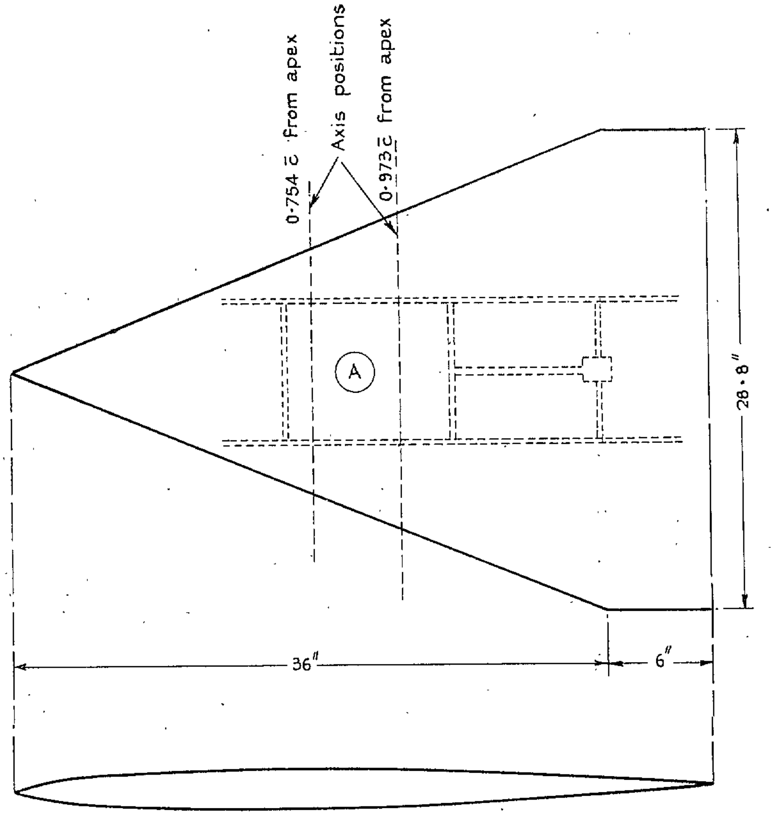

FIG. 1. The clipped delta wing (aspect ratio = 1·2).

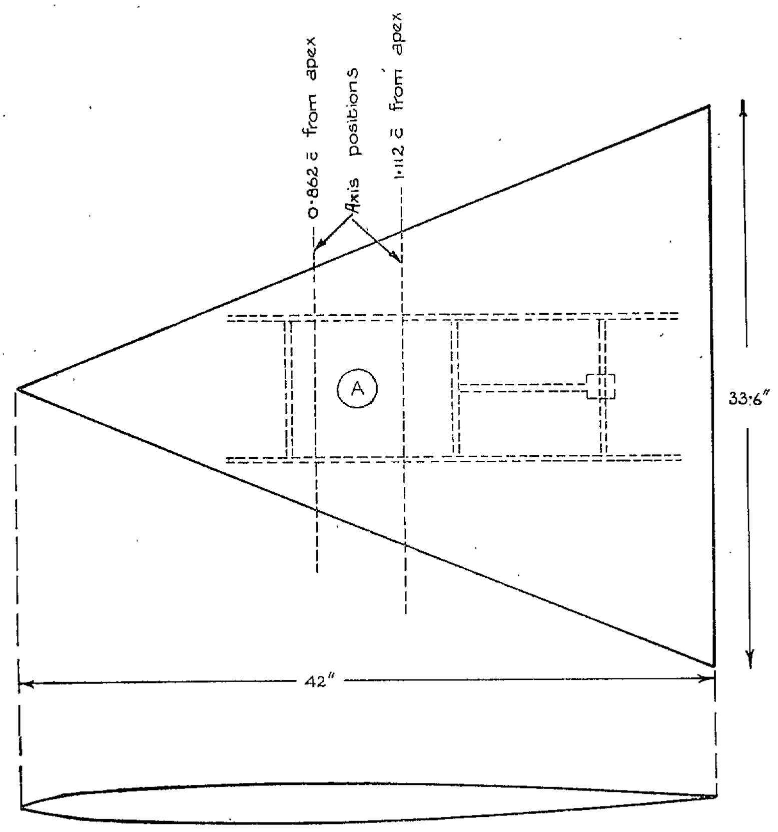

FIG. 2. The delta wing (aspect ratio = 1·6).

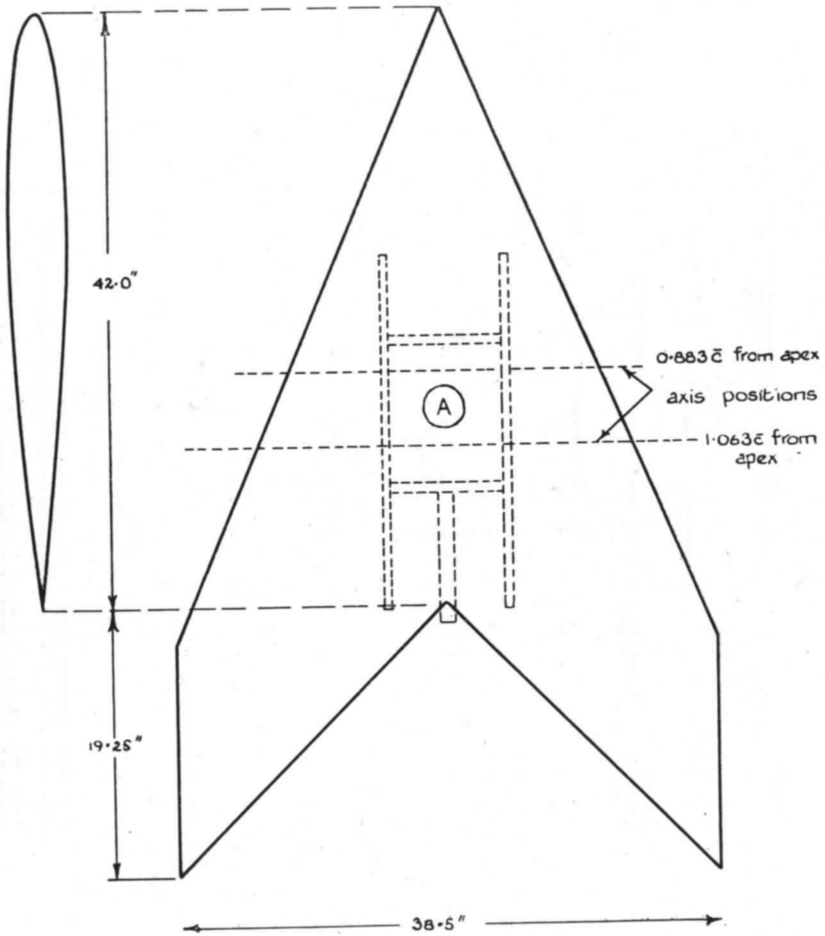

FIG. 3. The arrowhead wing (aspect ratio = 1·32).

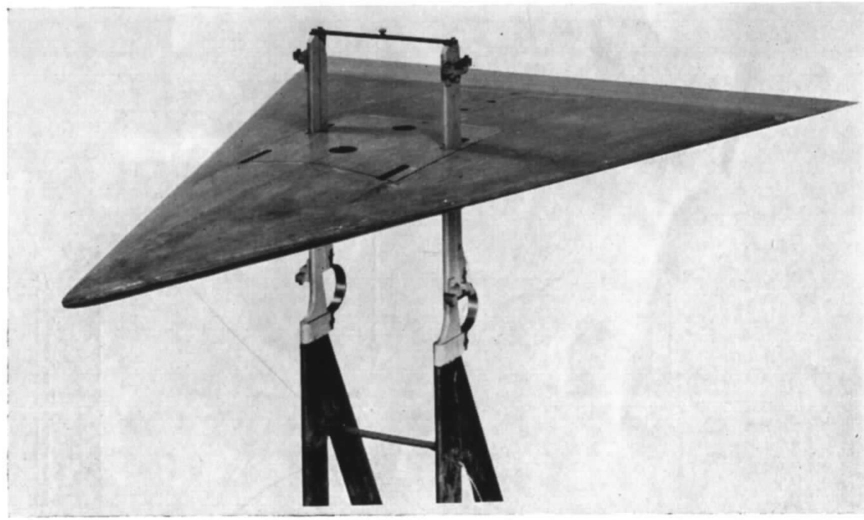

FIG. 4. View of the complete delta model mounted on the vertical force indicator.

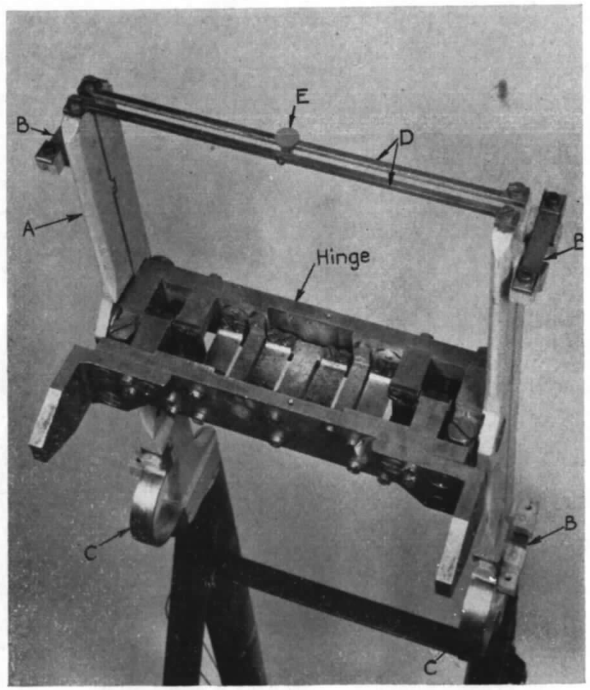

FIG. 5. Close-up view of the spring hinge mounted on the vertical force indicator.

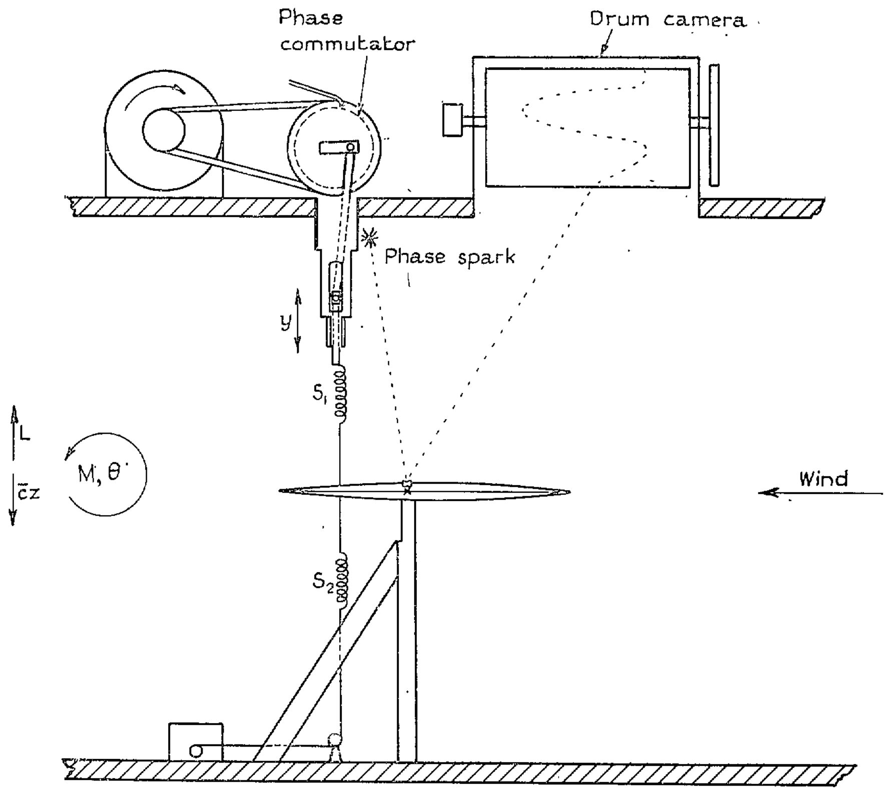

FIG. 6. Arrangement for measurement of pitching-moment derivatives.

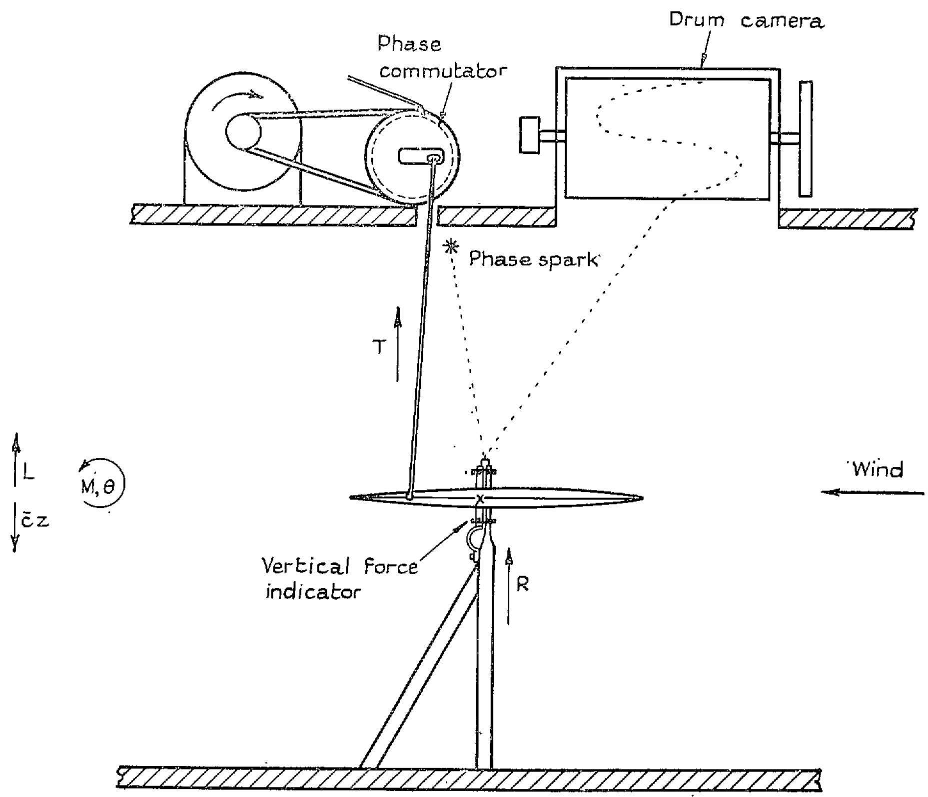

FIG. 7. Arrangement for measurement of lift derivatives.

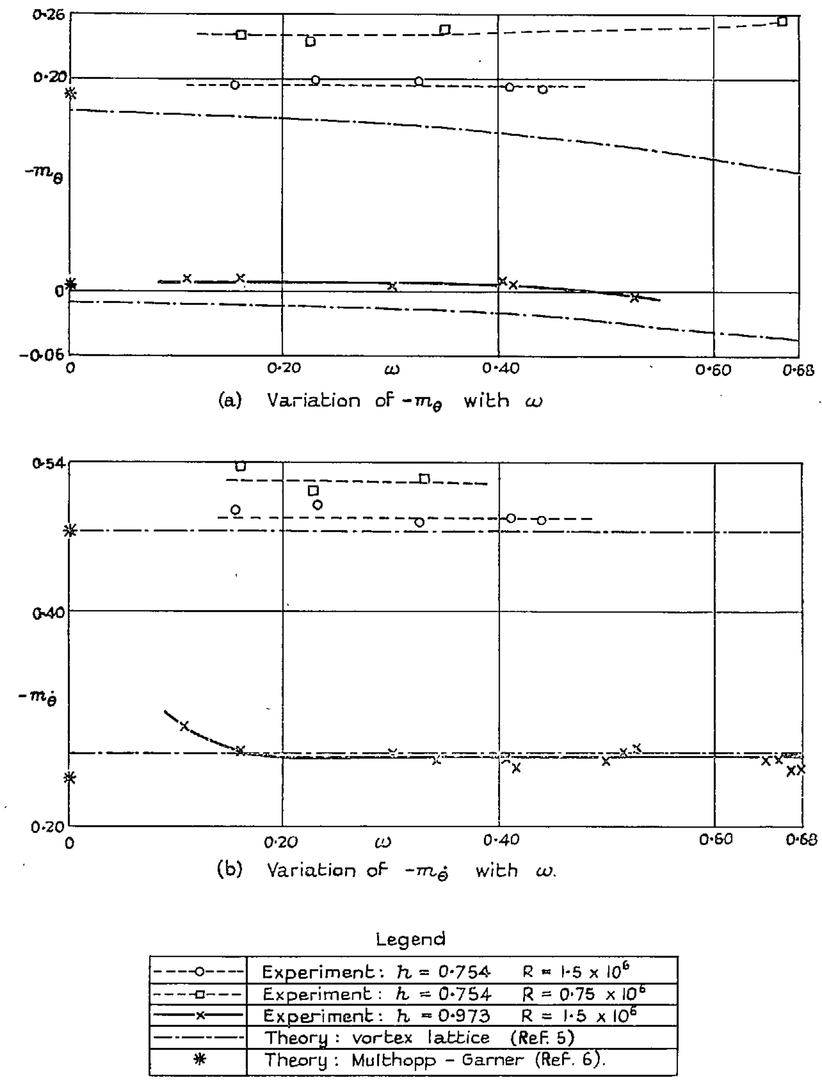

FIG. 8. Clipped delta wing. Aspect ratio = 1·2. Dependence of m_θ and $m_{\dot\theta}$ on ω for α = 0 deg.

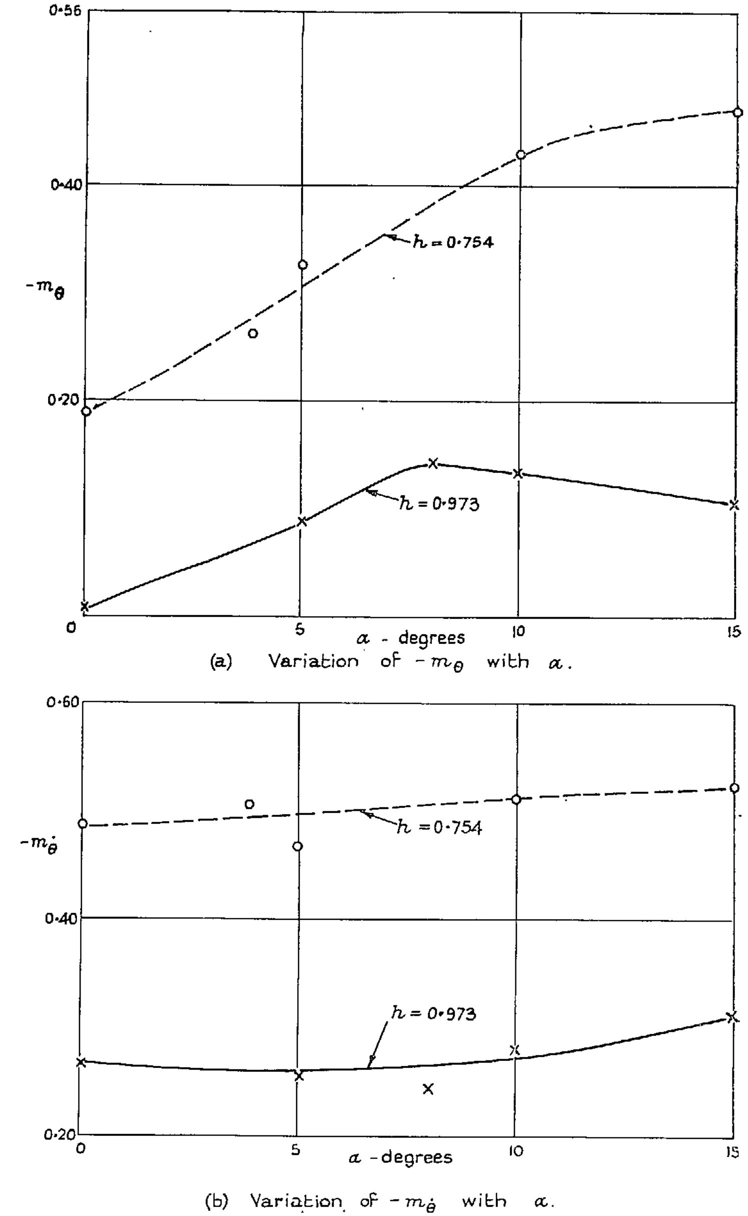

FIG. 9. Clipped delta wing. Aspect ratio = 1·2. Dependence of m_θ and $m_{\dot\theta}$ on ω for α = 0·3.

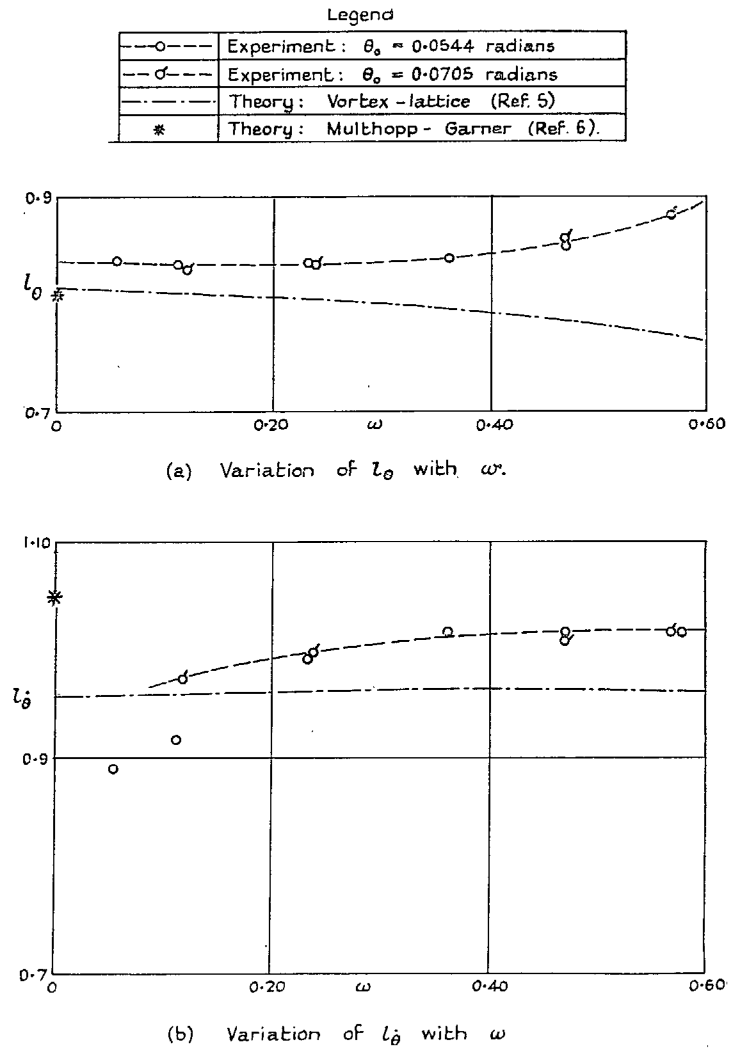

FIG. 10. Clipped delta wing. Aspect ratio $= 1 \cdot 2$. Dependence of l_θ and $l_{\dot\theta}$ on ω for $\alpha = 0$, $h = 0 \cdot 754$.

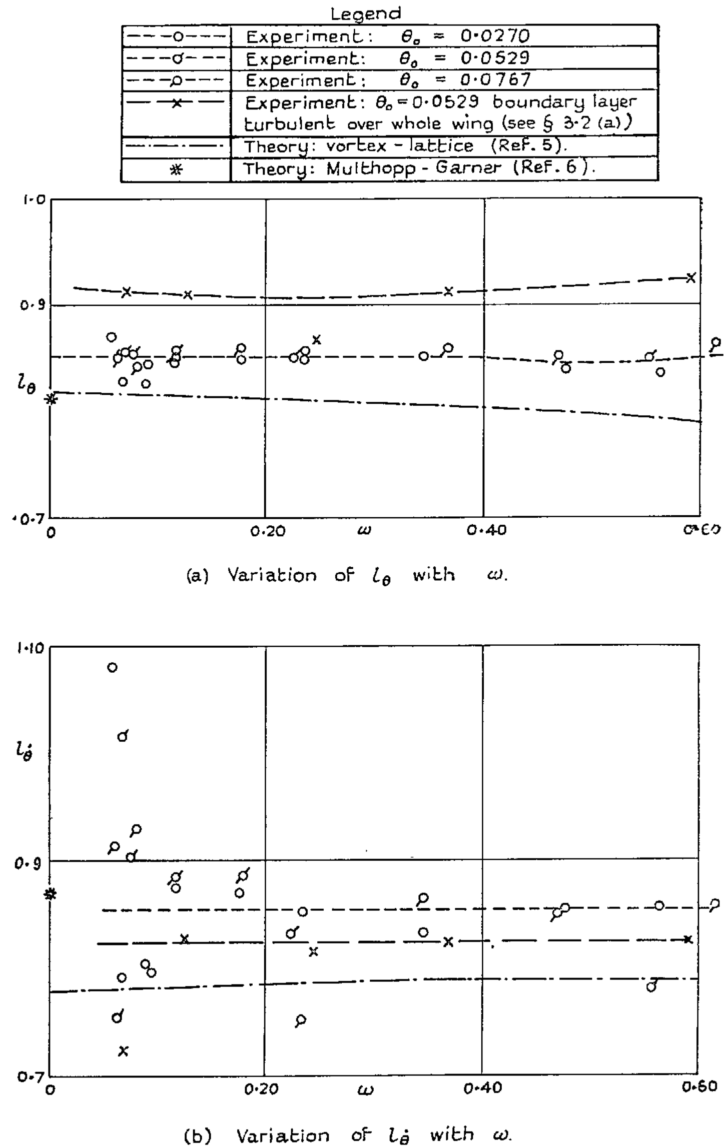

FIG. 11. Clipped delta wing. Aspect ratio $= 1 \cdot 2$. Dependence of l_θ and $l_{\dot\theta}$ on ω for $\alpha = 0$, $h = 0 \cdot 973$.

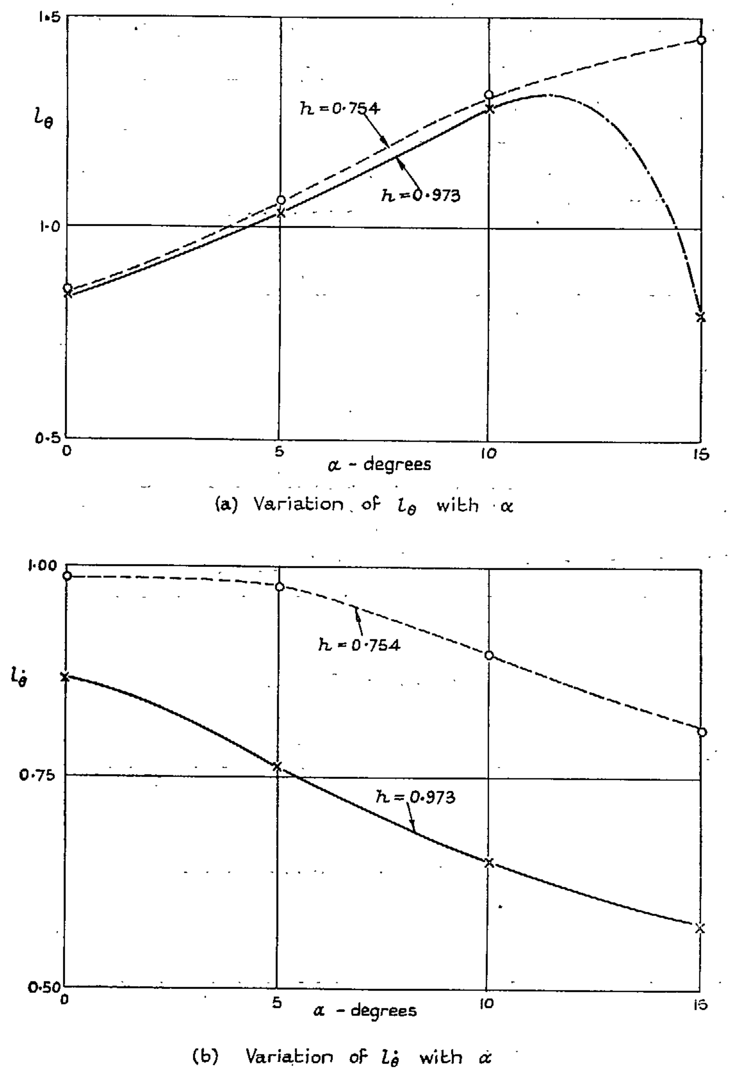

FIG. 12. Clipped delta wing. Aspect ratio $= 1{\cdot}2$. Dependence of l_θ and $l_{\dot\theta}$ on α for $\omega = 0{\cdot}3$.

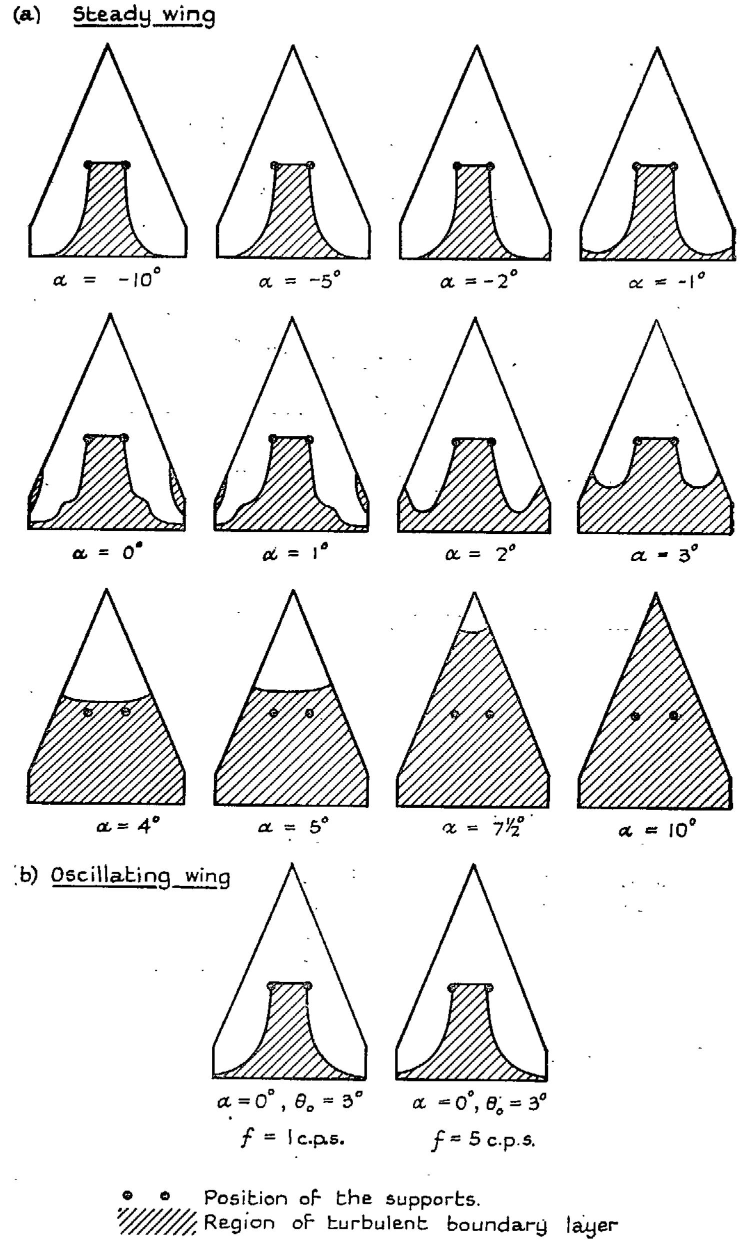

FIG. 13. Extent of the turbulent boundary layer on the upper surface of the clipped delta wing.

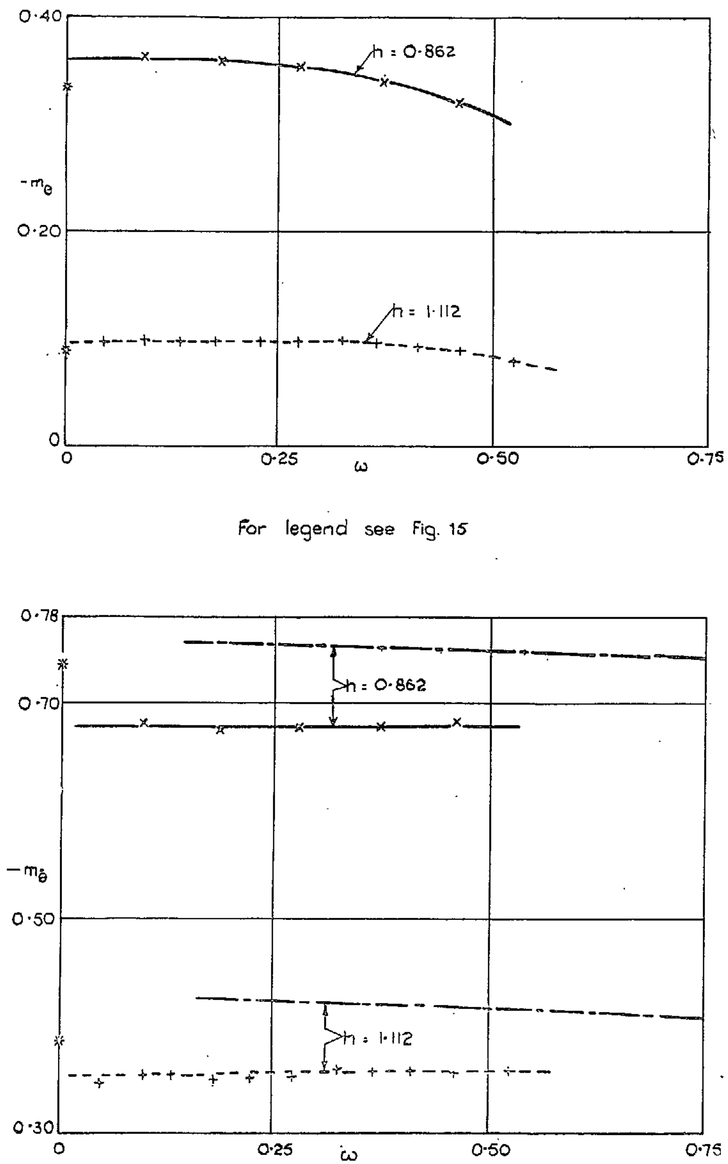

FIG. 14. Delta wing. Aspect ratio = 1·6. Dependence of m_θ and $m_{\dot\theta}$ on ω for $h = 0·862$ and $1·112$.

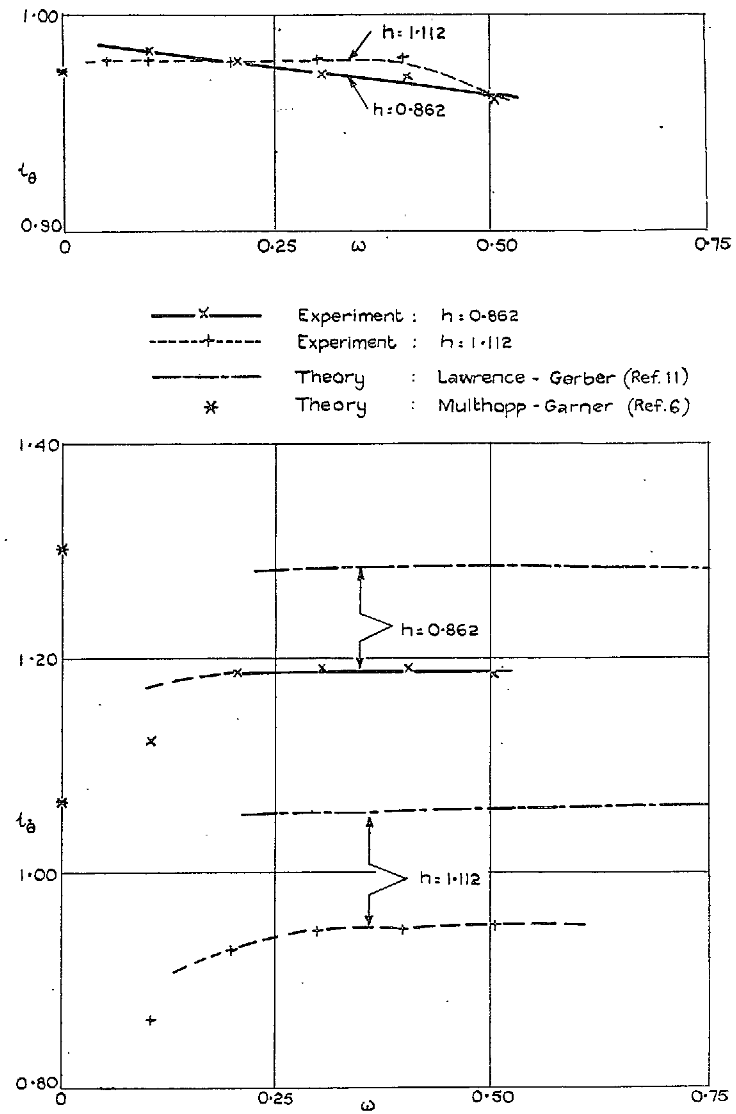

FIG. 15. Delta wing. Aspect ratio = 1·6. Dependence of l_θ and $l_{\dot\theta}$ on ω for $h = 0·862$ and $1·112$.

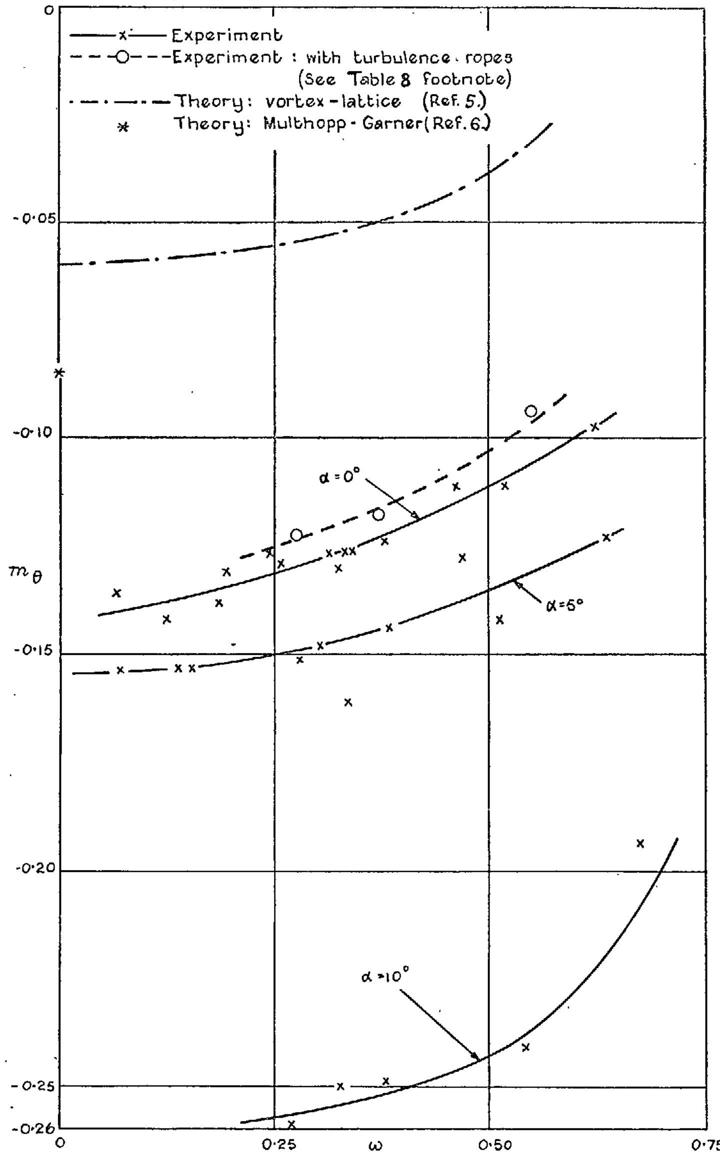

FIG. 16. Arrowhead wing. Aspect ratio = 1·32. Dependence of m_θ on ω and α for $h = 0 \cdot 883$.

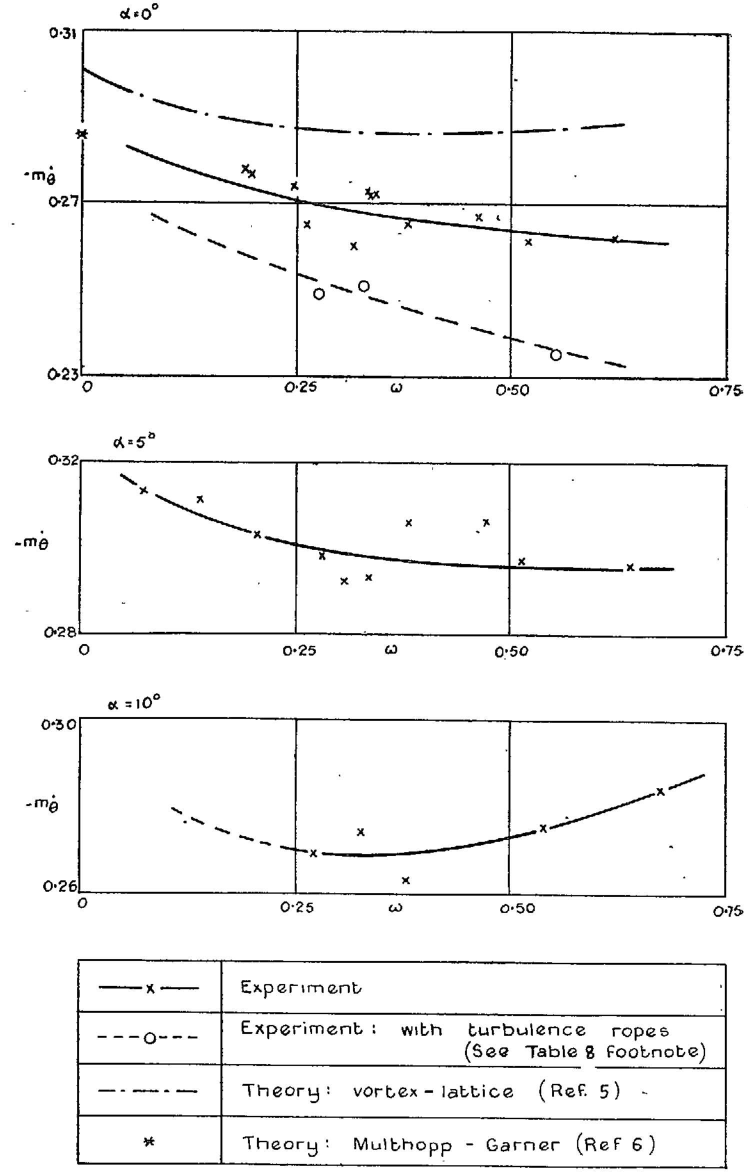

FIG. 17. Arrowhead wing. Aspect ratio = 1·32. Dependence of $m_{\dot\theta}$ on ω and α for $h = 0 \cdot 883$.

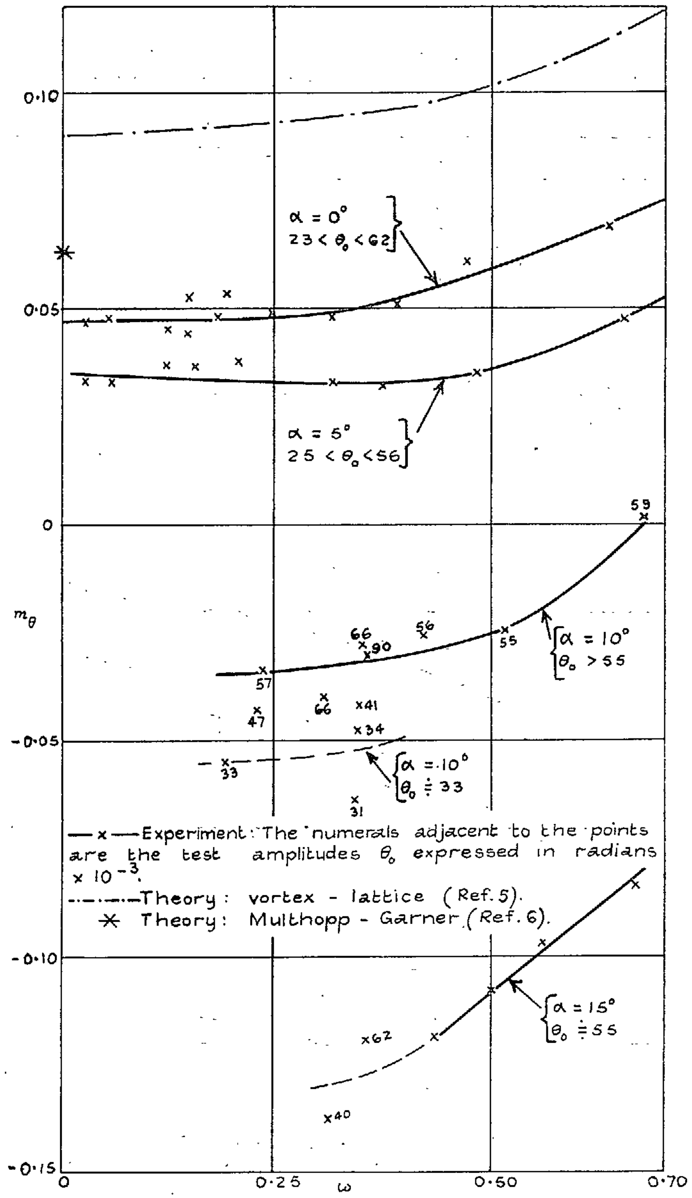

FIG. 18. Arrowhead wing. Aspect ratio = 1·32. Dependence of m_θ on ω and α for h = 1·063.

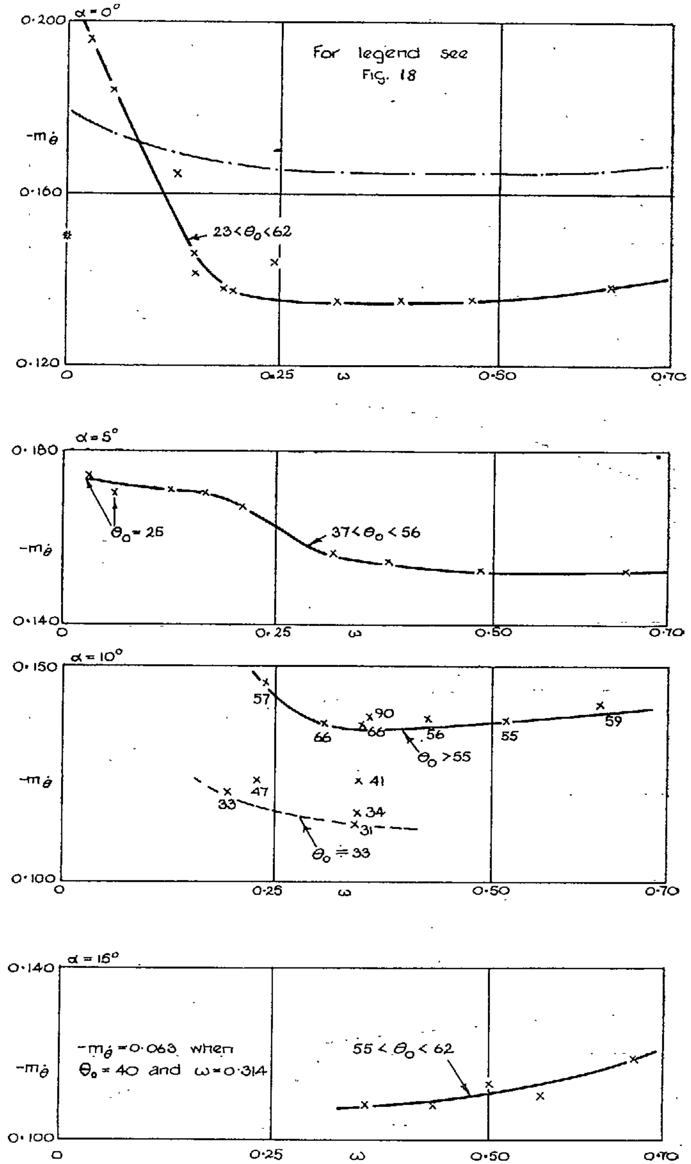

FIG. 19. Arrowhead wing. Aspect ratio = 1·32. Dependence of $-m_{\dot\theta}$ on ω and α for h = 1·063.

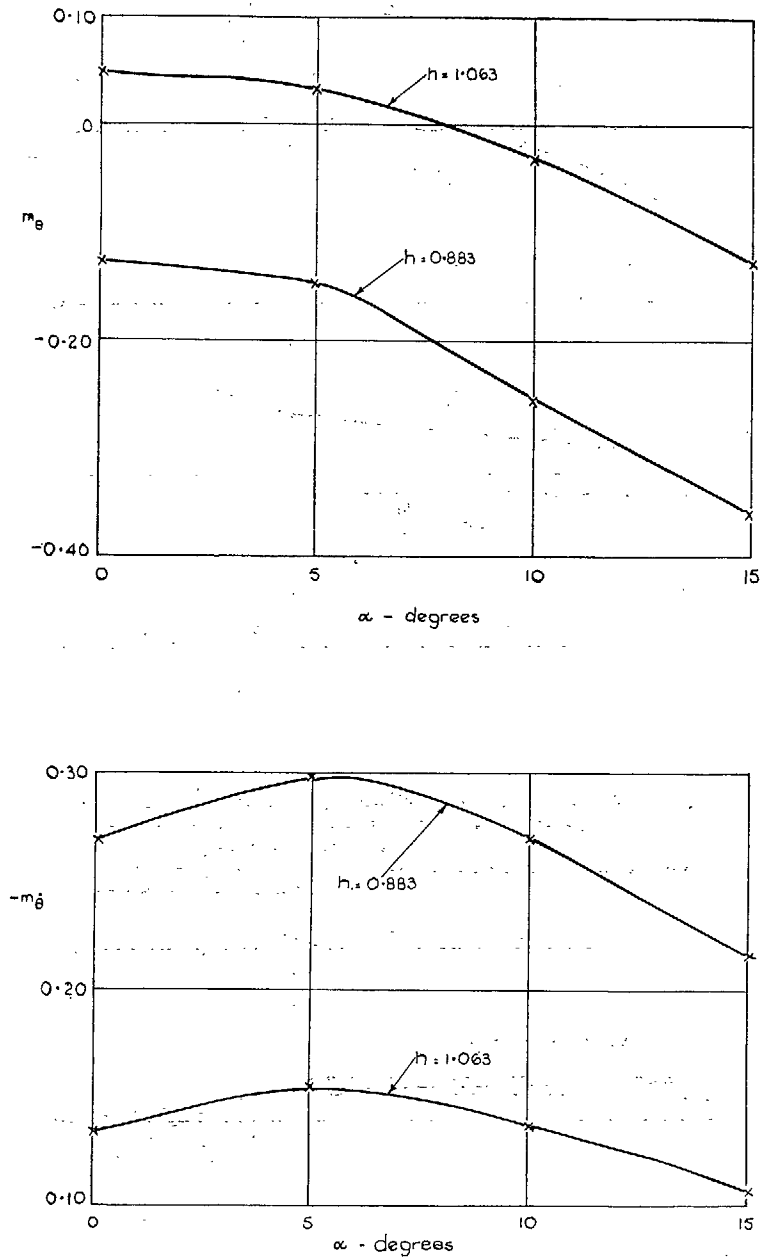

FIG. 20. Arrowhead wing. Aspect ratio = $1 \cdot 32$. Dependence of m_θ and $-m_{\dot\theta}$ on α and h for $\omega = 0 \cdot 3$.

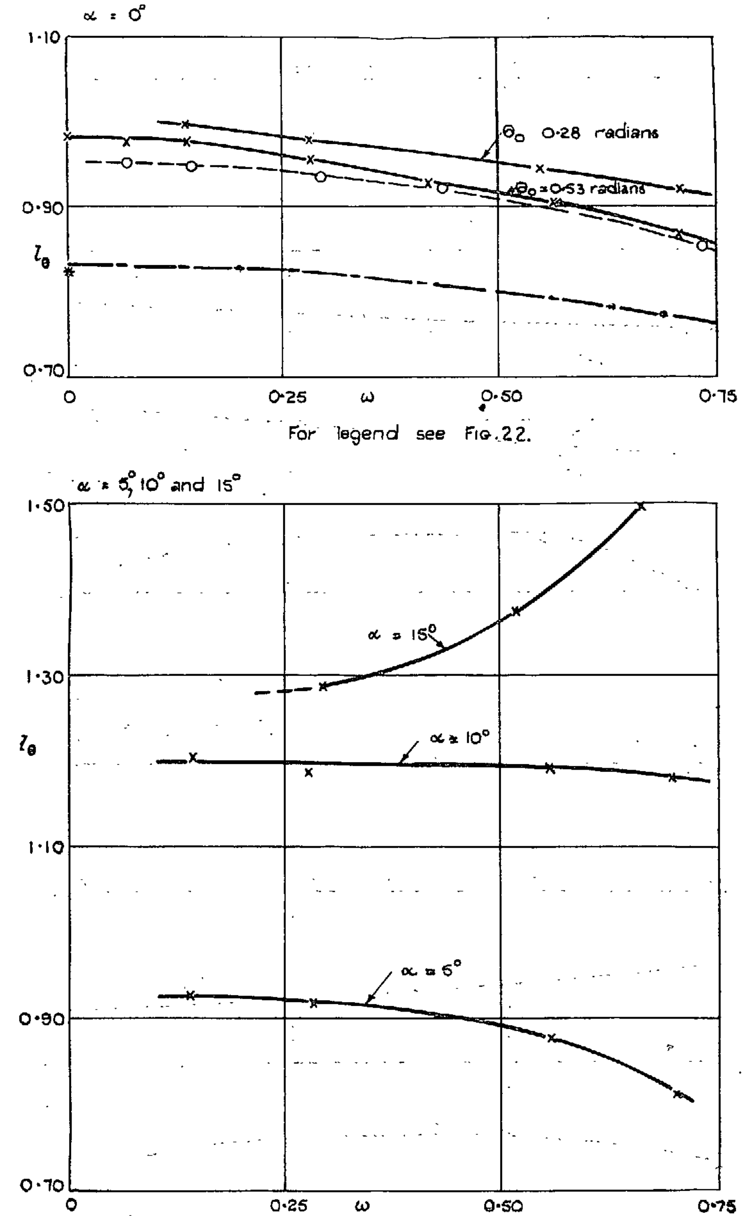

FIG. 21. Arrowhead wing. Aspect ratio = $1 \cdot 32$. Dependence of l_θ on ω and α for $h = 0 \cdot 883$.

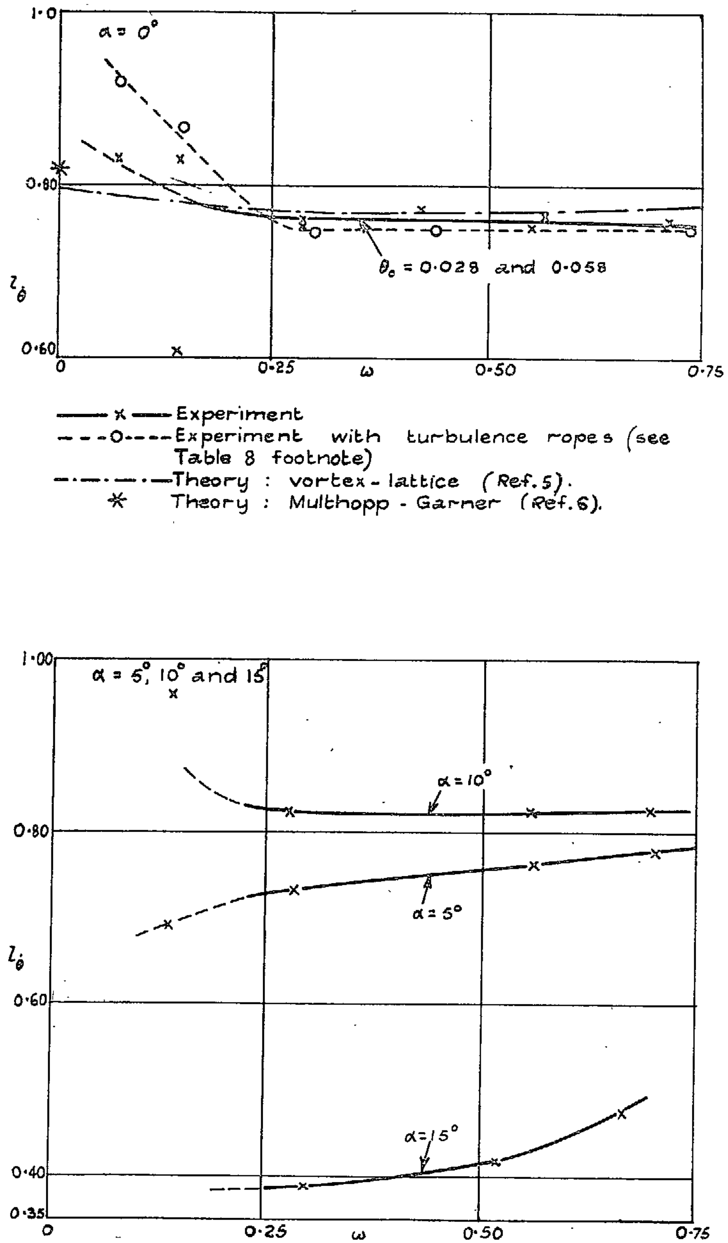

FIG. 22. Arrowhead wing. Aspect ratio = 1·32. Dependence of $l_{\dot\theta}$ on ω and α for $h = 0{\cdot}883$.

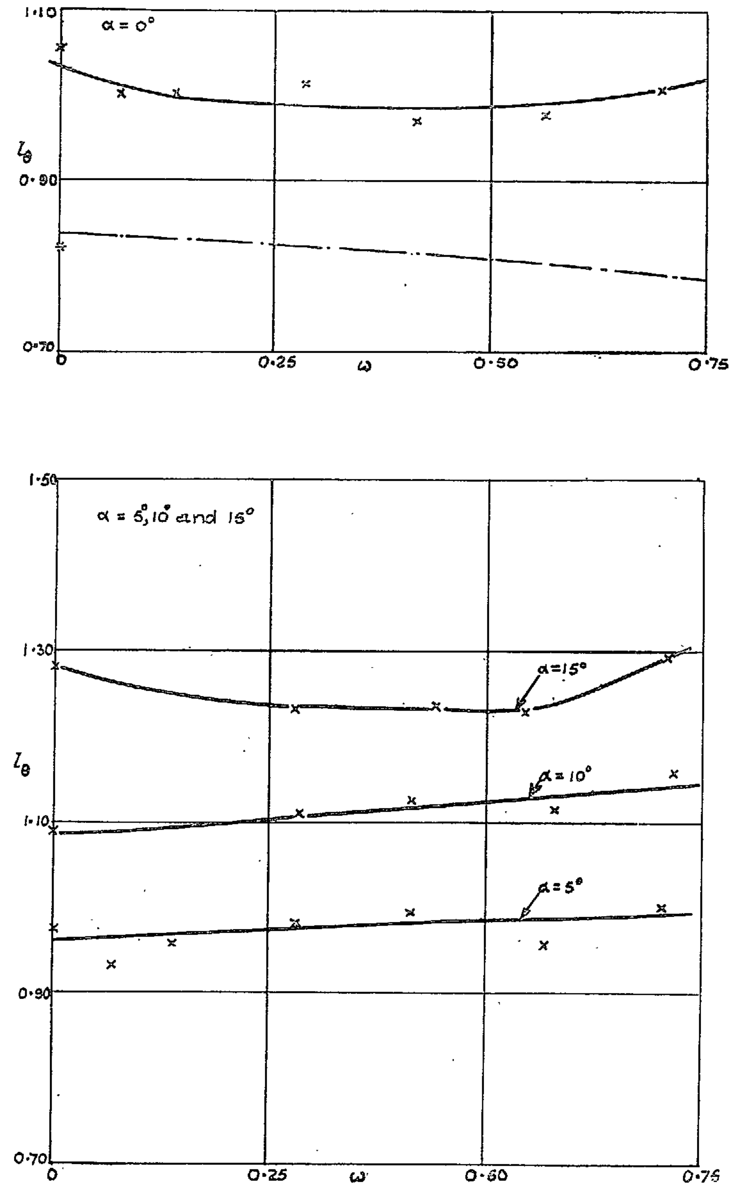

FIG. 23. Arrowhead wing. Aspect ratio = 1·32. Dependence of l_θ on ω and α for $h = 1{\cdot}063$.

J4349 Wt.19/8411 K7 9/55 D&Co. 34/263

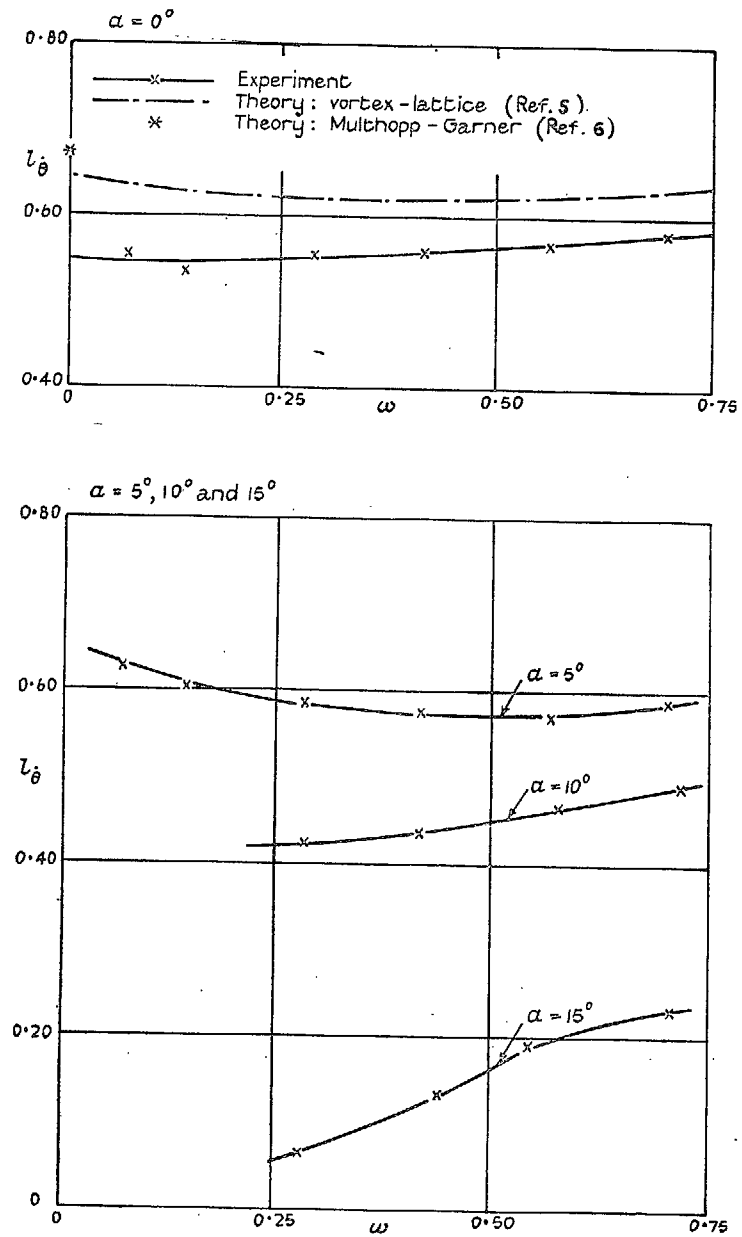

FIG. 24. Arrowhead wing. Aspect ratio = 1·32. Dependence of $l_{\dot{\theta}}$ on ω and α for $h = 1{\cdot}063$.

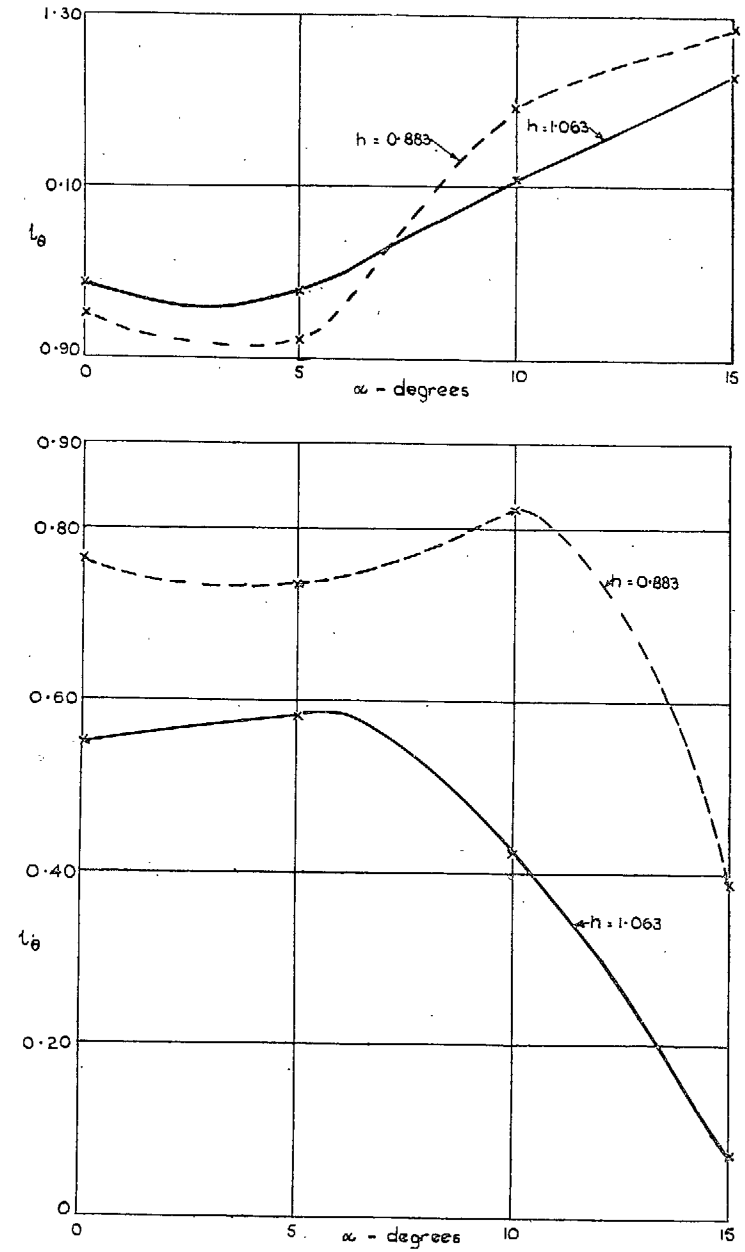

FIG. 25. Arrowhead wing. Aspect ratio = 1·32. Dependence of l_θ and $l_{\dot{\theta}}$ on α and h for $\omega = 0{\cdot}3$.

PRINTED IN GREAT BRITAIN

Publications of the Aeronautical Research Council

ANNUAL TECHNICAL REPORTS OF THE AERONAUTICAL RESEARCH COUNCIL (BOUND VOLUMES)

1939 Vol. I. Aerodynamics General, Performance, Airscrews, Engines. 50s. (51s. 9d.)
Vol. II. Stability and Control, Flutter and Vibration, Instruments, Structures, Seaplanes, etc. 63s. (64s. 9d.)

1940 Aero and Hydrodynamics, Aerofoils, Airscrews, Engines, Flutter, Icing, Stability and Control, Structures, and a miscellaneous section. 50s. (51s. 9d.)

1941 Aero and Hydrodynamics, Aerofoils, Airscrews, Engines, Flutter, Stability and Control, Structures. 63s. (64s. 9d.)

1942 Vol. I. Aero and Hydrodynamics, Aerofoils, Airscrews, Engines. 75s. (76s. 9d.)
Vol. II. Noise, Parachutes, Stability and Control, Structures, Vibration, Wind Tunnels. 47s. 6d. (49s. 3d.)

1943 Vol. I. Aerodynamics, Aerofoils, Airscrews. 80s. (81s. 9d.)
Vol. II. Engines, Flutter, Materials, Parachutes, Performance, Stability and Control, Structures. 90s. (92s. 6d.)

1944 Vol. I. Aero and Hydrodynamics, Aerofoils, Aircraft, Airscrews, Controls. 84s. (86s. 3d.)
Vol. II. Flutter and Vibration, Materials, Miscellaneous, Navigation, Parachutes, Performance, Plates and Panels, Stability, Structures, Test Equipment, Wind Tunnels. 84s. (86s. 3d.)

1945 Vol. I. Aero and Hydrodynamics, Aerofoils. 130s. (132s. 6d.)
Vol. II. Aircraft, Airscrews, Controls. 130s. (132s. 6d.)
Vol. III. Flutter and Vibration, Instruments, Miscellaneous, Parachutes, Plates and Panels, Propulsion. 130s (132s. 3d.)
Vol. IV. Stability, Structures, Wind tunnels, Wind Tunnel Technique. 130s. (132s. 3d.)

ANNUAL REPORTS OF THE AERONAUTICAL RESEARCH COUNCIL—

1937 2s. (2s. 2d.) 1938 1s. 6d. (1s. 8d.) 1939–48 3s. (3s. 3d.)

INDEX TO ALL REPORTS AND MEMORANDA PUBLISHED IN THE ANNUAL TECHNICAL REPORTS, AND SEPARATELY—

April, 1950 - - - - - R. & M. No. 2600. 2s. 6d. (2s. 8d.)

AUTHOR INDEX TO ALL REPORTS AND MEMORANDA OF THE AERONAUTICAL RESEARCH COUNCIL—

1909–January, 1954 - - - R. & M. No. 2570. 15s. (15s. 6d.)

INDEXES TO THE TECHNICAL REPORTS OF THE AERONAUTICAL RESEARCH COUNCIL—

December 1, 1936 — June 30, 1939.	R. & M. No. 1850.	1s. 3d. (1s. 5d.)
July 1, 1939 — June 30, 1945. -	R. & M. No. 1950.	1s. (1s. 2d.)
July 1, 1945 — June 30, 1946. -	R. & M. No. 2050.	1s. (1s. 2d.)
July 1, 1946 — December 31, 1946.	R. & M. No. 2150.	1s. 3d. (1s. 5d.)
January 1, 1947 — June 30, 1947. -	R. & M. No. 2250.	1s. 3d. (1s. 5d.)

PUBLISHED REPORTS AND MEMORANDA OF THE AERONAUTICAL RESEARCH COUNCIL—

Between Nos. 2251–2349. - -	R. & M. No. 2350.	1s. 9d. (1s. 11d.)
Between Nos. 2351–2449. - -	R. & M. No. 2450.	2s. (2s. 2d.)
Between Nos. 2451–2549. - -	R. & M. No. 2550.	2s. 6d. (2s. 8d.)
Between Nos. 2551–2649. - -	R. & M. No. 2650.	2s. 6d. (2s. 8d.)

Prices in brackets include postage

HER MAJESTY'S STATIONERY OFFICE

York House, Kingsway, London W.C.2; 423 Oxford Street, London W.1; 13a Castle Street, Edinburgh 2; 39 King Street, Manchester 2; 2 Edmund Street, Birmingham 3; 109 St. Mary Street, Cardiff; Tower Lane, Bristol 1; 80 Chichester Street, Belfast, *or through any bookseller*

S.O. Code No. 23-2925

R. & M. No. 2925